https://doi.org/10.5194/egusphere-2024-3048
Preprint. Discussion started: 23 October 2024

Intertidal Regions Regulate Seasonal Coastal Carbonate System Dynamics in the East Frisian Wadden Sea

Julia Meyer[1, 3], Yoana G. Voynova[1], Bryce Van Dam[1], Lara Luitjens[2], Dagmar Daehne[2], Helmuth Thomas[1, 3]

[1] Institute of Carbon Cycles, Helmholtz-Zentrum Hereon, Geesthacht, 21502, Germany
[2] Lower Saxony department of water management, coastal protection and nature protection (NLWKN), Norden, 26506, Germany
[3] Institute for Chemistry and Biology of the Marine Environment (ICBM), Carl von Ossietzky Universität Oldenburg, 26111 Oldenburg, Germany

Correspondence to: Julia Meyer (julia.meyer@hereon.de)

Abstract. Seasonal and regional changes in carbon dynamics in the Wadden Sea, the world´s largest intertidal sand and mud flats system, were analyzed to quantify the influence of biogeochemical processes ($CaCO_3$ dissolution and formation, photosynthesis, respiration) on the carbonate system at the land-sea interface. With a focus on the East Frisian Wadden Sea and the highly turbid Ems River estuary, we successfully implemented the proxy of the difference between total alkalinity (TA) and dissolved inorganic carbon (DIC) ([TA-DIC]), as well as the calculated ΔTA_{excess}, ΔDIC_{excess} and ΔTA_P to identify how ongoing biogeochemical processes regulate the carbonate system dynamics and the land-sea interface.

In spring, a phytoplankton bloom with high biological activity was indicated by (a) supersaturated oxygen (up to 180 in % saturation), (b) elevated chlorophyll a (up to 151.7 µg L^{-1}) and (c) low pCO_2 (as low as 141.3 µatm). As a result, nitrate (NO_3^-, 19.29 ± 18.11 µmol kg^{-1}) and DIC (159.4 ± 125.4 µmol kg^{-1}) decreased, whereas TA slightly increased (9.1 ± 29.2 µmol kg^{-1}) in the intertidal regions from March 2022 to May, most likely through nitrate assimilation. The regression analysis of the differences in NO_3^- concentrations (ΔNO_3^-) against the differences in DIC (ΔDIC) between March and May 2022 yielded a slope of 6.90 which is close to the Redfield ratio of 6.625 for the C:N ratio of freshly produced phytoplankton biomass.

In summer, high seasonal TA values (up to 2400 µmol kg^{-1}) in the Western part of the East Frisian Wadden Sea, along with positive ΔTA_{excess} at 73.3 % of all stations, indicated production of TA during this season in the intertidal regions, complemented the DIC dynamics. The increase of TA enhances the coastal ocean's ability to absorb and store CO_2 through buffering, chemical equilibrium, biological calcification and the carbonate pump, and suggests that the intertidal regions can be a source of total alkalinity to the coastal regions during the warm productive seasons. The study highlights the complex relationships of these factors, emphasizing the need for a comprehensive understanding of regional and seasonal variations to better assess the role of coastal systems in carbon cycling, storage and climate regulation.

https://doi.org/10.5194/egusphere-2024-3048
Preprint. Discussion started: 23 October 2024

1 Introduction

Coastal oceans are biogeochemically active regions, which play a significant role in biogeochemical cycles, despite covering less than 10 % of the oceanic realm (Gattuso et al., 1998). Coastal regions are directly affected by input of terrestrial organic matter and nutrients through river run-off and groundwater discharge and atmospheric deposition, with exchange of large amounts of matter and energy with the open ocean (Borges et al., 2006; Gattuso et al., 1998). Overall, coastal oceans also support approximately 14 - 23 % of the ocean carbon dioxide uptake, 10 - 30 % of the primary production, 80 % of organic matter burial, 90 % of sedimentary mineralization and 75 - 90 % of the oceanic sink of suspended river loads (Bauer et al., 2013; Gattuso et al., 1998).

For years, the levels of CO_2 in the atmosphere have been increasing from ~280 ppm in the preindustrial period to over ~ 419 ppm due to human activities (Friedlingstein et al., 2023). The uptake of atmospheric CO_2 by the ocean, estimated to about 30 % of the anthropogenic emissions since the industrial period (Friedlingstein et al., 2023), causes an increase in protons [H^+] and a decrease of carbonate ion concentration [CO_3^{2-}], which lower the pH and saturation state of calcium carbonate, a process known as ocean acidification (Orr et al., 2005). Depending on the different model scenarios, it is predicted that surface pH in the ocean might decline by about 0.3 – 0.4 pH units by 2100, corresponding to a decrease of about 40 – 50 % of carbonate ions in the seawater (Feely et al., 2009; Orr et al., 2005). The future capacity of the ocean to take up CO_2, can affect the precipitation and dissolution of the carbonate minerals, as well as the survival of marine organisms (Kroeker et al., 2013). Whereas oceans are a significant sink for anthropogenic CO_2, it is not well known how this uptake will further change under the continual increase of anthropogenic CO_2 in the atmosphere (Sabine et al., 2004). However, rising atmospheric CO_2 will influence carbon stocks and fluxes in the pelagic, benthos and coastal zone, particularly in shelf seas, which are annually mixed and ventilated (Legge et al., 2020).

Total alkalinity (TA) represents the buffering capacity of the ocean and is controlled by many factors including erosion/weathering processes on land (Lehmann et al., 2023) and respiration of organic matter (OM) along anaerobic metabolic processes, mostly generated in shallow marine and shelf sediments (Dickson, 1981). These processes are directly influenced by terrestrial and anthropogenic nutrient inputs (Van Beusekom and De Jonge, 2002; Burt et al., 2016; Thomas et al., 2009) and by increased sedimentation of reactive organic matter (OM) (Al-Raei et al., 2009; Böttcher et al., 1998). Coastal seas and shelf seas, like the North Sea often have relatively high rates of primary production in spring, leading to drawdown in DIC, pCO_2 and a consequent pH increase (Macovei et al., 2021; Thomas et al., 2005a). In addition, nutrient loads from land can contribute to enhanced primary production, and increased carbon remineralization (Thomas et al., 2009), and subsequent changes in the carbonate system. In addition, there have been studies (Thomas et al., 2009; Voynova et al., 2019), which suggest that intertidal regions like the Wadden Sea can play a significant role in modulating local carbonate system dynamics (Voynova et al., 2019). The seasonal TA production, which ranged between 11.7 - 26.8 mmol m^{-2} d^{-1} in the spring and summer months and exhibited a regional TA variability of up to 100 µmol kg^{-1}, was attributed to the influence of the extensive sand and mudflats in the Wadden Sea (Voynova et al., 2019), and benthic TA production (Brenner et al., 2016). The observed

https://doi.org/10.5194/egusphere-2024-3048
Preprint. Discussion started: 23 October 2024

changes of TA can affect the coastal ocean capacity to absorb carbon from the atmosphere (Burt et al., 2016; Gruber et al., 2019; Li et al., 2024; Schwichtenberg et al., 2020).

The current study focuses on seasonal and inter-annual changes in and around the coastal, tidally driven East Frisian Wadden Sea, aiming to identify the sources of TA and DIC responsible for the previously observed seasonal increase in adjacent coastal regions. We conducted seasonal cruises and combined underway FerryBox measurements, carbonate system measurements and nutrient data to characterize the effect of primary production and nutrient cycling on TA generation and carbon dynamics in the East Frisian Wadden Sea. The resultant regional and seasonal distributions of TA and DIC contribute to the elucidation of the potential sources of carbon and TA in this region.

2 Material and Methods

2.1 Study Side

The German Bight region is bordered by Germany, Denmark and the Netherlands, and is situated in the southeastern corner of the North Sea (Fig. 1a). The East Frisian Wadden Sea is one of the shallowest regions of the German Bight, characterized by a series of barrier islands, each 5 – 17 km long and 2 – 3 km wide (Staneva et al. 2009). The system is influenced by semidiurnal tides with a tidal range from approximately 2.2 - 2.8 m (Grunwald et al. 2009; Staneva et al. 2009) and up to ~ 3.5 m in the Elbe River mouth (Staneva et al. 2009). Seasonal cruises were completed in the Wadden Sea (WS) and North Sea around the East Frisian Islands and the Ems River estuary on the research vessel (RV) "*Burchana*" (Lower Saxony department of water management, coastal protection, and nature protection (NLWKN; Fig. 1). The cruises in July 2021 and October 2021 were carried out only in the intertidal East Frisian WS. Later cruises were extended to the Ems River Estuary, from the weir in Herbrum to the island of Borkum (Bork, Fig. 1b); the Ems drains a catchment area of about 12,600 km^3 (Talke and De Swart 2006). Samples were taken following the salinity gradient up to Weener with a salinity of ~ 0 in the Ems River estuary.

https://doi.org/10.5194/egusphere-2024-3048
Preprint. Discussion started: 23 October 2024

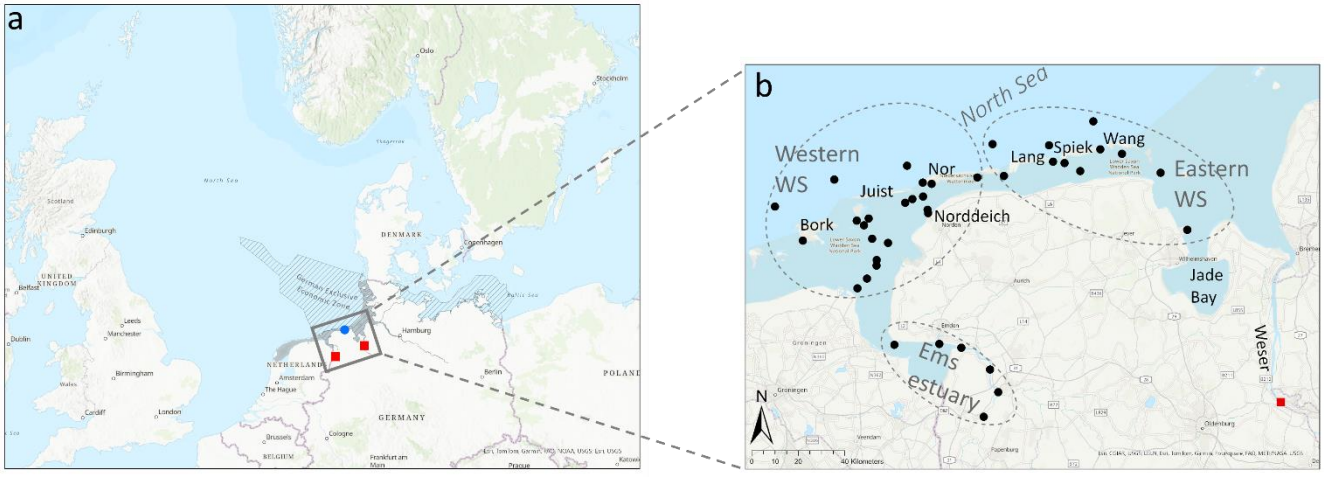

Figure 1: Study area, (a) The German Wadden Sea (=WS), (shown in grey) with the German Exclusive Economic Zone (hatched region) and the East Frisian WS region (grey box). (b) Zoom into the East Frisian WS, showing the sampling stations (black dots) in the different regions in the East Frisian WS (Western WS and Eastern WS) considered in this study. The different Islands are labeled with their first letters (Bork= Borkum, Juist, Nor= Norderney, Lang= Langeoog, Spiek= Spiekeroog, Wang= Wangeoog). The red squares show the inflow of the Ems and Weser Rivers into their estuaries. The blue point shows the location of the sluice in Neuharlingersiel. The map in this Figure was generated using ArcGIS. Data sources: Esri, TomTom, Garmin, FAO, NOAA, USGS. © 2024 Julia Meyer.

2.2 FerryBox measurements

A FerryBox system (4H-JENA engineering GmbH, Jena, Germany) operated during all cruises of the *RV Burchana* (NLWKN), measuring the following parameters every minute: temperature (SBE38, Sea-Bird Scientific), salinity (SBE45, Sea-Bird Scientific), dissolved oxygen (DO) (Optode 4835, Aanderaa, Bergen, Norway), chlorophyll fluorescence to estimate chlorophyll a concentrations (AlgaeOnlineAnalyser, bbe moldaenke), pH (electrode, Xylem), turbidity (Solitax inline SC, Hach Lange) and partial pressure of CO_2 (pCO_2) (4H-JENA engineering). The data were corrected using the data processing manual of 4H - Jena engineering GmbH (4H Jena, 2021). Regions near the ports were excluded in all datasets, to remove any influence of the ship in port, or from the cleaning cycles. Chlorophyll a was not measured in March and May 2022 in the whole Ems River estuary, due to interference by turbidity in the hyper turbid Ems River estuary (Schulz et al. 2022). Samples for Winkler titration (dissolved oxygen), nutrients, salinity and turbidity were collected from each cruise from October 2021 and until July 2022 to crosscheck the measurements of the FerryBox.

2.3 Discrete samples

Dissolved oxygen (DO) samples were collected on the last day of each cruise from October 2021 until July 2022 by filling Biological Oxygen Demand (BOD) bottles from the FerryBox outflow for at least one minute with water overflow to remove any bubbles. Three replicates at each station were collected and 2 mL of each manganese sulfate and alkali-iodide-azide reagents were pipetted in each sample just below the surface of the liquid, with care that no bubbles were introduced. Each

https://doi.org/10.5194/egusphere-2024-3048
Preprint. Discussion started: 23 October 2024

BOD bottle was carefully stoppered and mixed by inverting the sample several times. All DO samples were measured within 24 hours of collection in the lab with a Metrohm 870 KF Titrino Plus.

The Winkler titrations were used to correct the FerryBox dissolved oxygen measurements from the seasonal cruises. A single regression equation for the Winkler oxygen and the FerryBox data was used to apply a salinity and temperature correction of the entire data set ($y= 1.17x - 31.89$, $R^2= 0.98$, $n= 46$). In addition, the apparent oxygen utilization (AOU) was calculated from all corrected oxygen measurements, which is defined as:

$$AOU= O_2^{'} - O_2 \quad (1)$$

Where O_2' is the expected oxygen at equilibrium with the atmosphere, at given temperature and salinity according to Grasshoff et al., (1999) in µmol L^{-1}, whereas O_2 is the oxygen concentration measured by the FerryBox optode 4835, in µmol L^{-1}.

Duran bottles (~ 300 mL) were filled with sample water during all seasonal sampling cruises using the FerryBox outflow to measure turbidity and salinity in the laboratory. The samples were capped tightly and measured within a few days of collection in the laboratory. Turbidity in the lab was measured with a Hach Turbidimeter 2100. Salinity was measured with an OPTIMARE High Precision Salinometer (Optimare Systems GmbH, Bremerhaven, Germany). The turbidity and salinity lab measurements were used to quality control the FerryBox measurements.

The nutrient water samples were taken directly with the water sampler on board of the *RV Burchana* at each station (Fig. 1). A sample volume of 250 mL was filtered using pre-combusted GF/F filters, the samples were collected in clean centrifuge tubes, which was frozen and stored at -20°C. Nitrite (NO_2^-), nitrate (NO_3^-) ammonium (NH_4^+) and silicate (SiO_2) concentrations were also measured via MicroMaC analyzer from SYSTEA (Anagni (FR), Italy). The system is located on board of the *RV Burchana* (NLWKN), inducing a color reaction, coupled with a photometer (NO_3^-, NO_2^-, SiO_2) and fluorometer (NH_4^+), using a one-point calibration. Distilled ultrapure water was used for the automatically aspirated dilutions. NO_3^- was determined with sulfanilamide and N- (1- Naphthyl)ethylenediamine, NH_4^+ with orthophthalaldehyde and NO_2^- with diethylenetriaminepentaacetic acid and automatic UV reduction (Luitjens, 2019). Silicium reacts with molybdic acid in acidic media to form yellow heteropoly acids. Upon reduction in a strongly acidic solution, a deep blue reaction product, referred to as "silicomolybdic blue," is obtained (Luitjens, 2019).

Water samples for TA and DIC were collected in 300 mL BOD bottles at all stations using the FerryBox outflow according to the Standard Operating Procedure (SOP) for carbonate system sample collection (Dickson et al. 2007). The samples were poisoned with saturated mercury chloride solution in order to stop any biological activity. The samples were stored in the dark, at room temperature, and measured in the laboratory with a VINDTA 3C (MARIANDA, Kiel, Germany), and calibrated using certified reference material (CRM) (Dickson et al. 2003). The results within this study were plotted with R Project (ggplot package) and maps were created with ArcGIS Pro. In addition, the saturation state of calcite (Ωcal) calculated using the CO2SYS program developed by (Lewis et al. 1998) with CO_2 solubility constants of Lueker et al. (2000).

https://doi.org/10.5194/egusphere-2024-3048
Preprint. Discussion started: 23 October 2024

2.4 Temperature normalized pCO_2 estimation

Changes in temperature influence the pCO_2 value of surface waters by controlling the thermodynamic equilibrium of the inorganic carbon system (Takahashi et al. 1993) and thus is affected by seasonal changes (Takahashi et al. 2002). To calculate the thermal component ($pCO_{2\ therm}$) of the observed pCO_2 ($pCO_{2\ obs}$) the equation of Takahashi et al. (1993) was used:

$$pCO_{2\,\mathrm{therm}} = pCO_{2_{\mathrm{obs\ Mean}}} * \exp[0.0423 * (T_{obs} - T_{Mean})] \quad (2)$$

$pCO_{2\ obs\ Mean}$ is the annual mean pCO_2 observed, and T_{Mean} is the annual mean surface temperature over the year. The biological component was also calculated (Takahashi et al. 1993; Kitidis et al. 2019):

$$pCO_{2\,\mathrm{bio}} = pCO_{2_{\mathrm{obs}}} * \exp[0.0423 * (T_{Mean} - T_{obs})] \quad (3)$$

2.5 Calculations of estuarine DIC and TA contributions

The separation of the different regions within the East Frisian WS allows to use to different riverine endmember for each defined region. For the Western WS we used the measured DIC values of the Ems River estuary with the lowest measured salinity to estimate DIC_{river} in March, May and July 2022. In July 2021 we used the results of discrete samples at the Herbrum Wehr, taken in August 2021 and in October 2021, the discrete samples from the end of October 2021 (Table 1). For the Eastern WS, the Weser River (Fig. 1, marked in red) was used to calculate an average of DIC_{river} (Table 1). Therefore, the Weser River was sampled in August 2021, October 2021 and April 2022.

Table 1: DIC_{river}, DIC_{ocean}, S_{ocean}, TA_{river} and TA_{ocean} used for the calculation of the seasonal $DIC_{mixing\ w/R}$ concentrations of each season.

Season and Region	DIC_{river}	DIC_{ocean}	S_{ocean}	TA_{river}	TA_{ocean}
July 2021					
Eastern WS	2701.7	2119.8	32.05	2435.7	2273.7
Western WS	2491.9	2152.5	31.50	2541.1	2365.2
October 2021					
Eastern WS	2577.2	2188.5	30.63	2467.9	2369.3
Western WS	2418.7	2176.4	30.97	2321.6	2378.7
March 2022					
Eastern WS	2647.2	2205.7	31.47	2205.7	1824.8
Western WS	2785.2	2187.9	29.92	2187.9	2622.9
May 2022					
Eastern WS	2647.2	2119.9	32.13	1824.8	2332.5
Western WS	2864.1	2084.5	31.6	2722.5	2351.2
July 2022					
Eastern WS	2647.2	2144.4	31.78	1824.2	2356.6
Western WS	2929.3	2173.9	32.03	2853.7	2396.6

The influence of the riverine input can affect the carbon dynamics, especially in a shelf sea such as the North Sea. In this study we used the equation of (Jiang et al. 2008; Joesoef et al. 2015) to calculate $DIC_{mixing\ w/R}$:

$$DIC_{\mathrm{mixing\ w/R}} = \frac{S_i}{S_{ocean}} + DIC_{ocean} + (1 - \frac{S_i}{S_{ocean}}) * DIC_{river} \quad (4)$$

https://doi.org/10.5194/egusphere-2024-3048
Preprint. Discussion started: 23 October 2024

which is the DIC concentration after mixing of the DIC concentration of the nearshore regions (DIC_{ocean}) and the DIC concentration of the riverine endmember Weser and Ems (DIC_{river}). The S_i and S_{ocean} are the salinity concentrations of the station *i* and the North Sea endmember (nearshore regions) with the seasonal highest salinity measured in the Western and Eastern regions.

In Addition, the ΔDIC_{excess} was calculated to estimate the contribution due to riverine input in the different regions. Therefore, the equation of (Van Dam et al., 2018; Jiang et al., 2008) was used:

$$\Delta DIC_{excess} = DIC_i - DIC_{mixing\ w/R} \quad (5)$$

This equation includes the measured DIC concentrations of the related station *i* and the $DIC_{mixing\ w/R}$.of equation 4. $\Delta TA_{mixing\ w/R}$.and ΔTA_{excess} were calculated the same way with the measured TA of each station using the TA_{river}, TA_{ocean} concentations (Table 1):

$$TA_{mixing\ w/R} = \frac{S_i}{S_{ocean}} + TA_{ocean} + (1 - \frac{S_i}{S_{ocean}}) * TA_{river} \quad (6)$$

$$\Delta TA_{excess} = TA_i - TA_{mixing\ w/R} \quad (7)$$

ΔDIC_{excess} and ΔTA_{excess} concentrations were calculated to remove mixing effect of the rivers with the sea. The coastal region of the East Frisian WS is closely connected to the land and the rivers are usually supersaturated with CO_2compared to the atmosphere (Joesoef et al. 2015). A ΔDIC_{excess} value of approximately zero means that the DIC is not different than what would be expected upon mixing between the ocean and river. Negative values of ΔDIC_{excess} confirm that the DIC consumption exceeded production in this area, which reduces DIC or, equivalently increases ΔTA_{excess}. Positive values of ΔTA_{excess} suggests higher values than expected based on mixing alone, indicating other additional TA sources are present, caused for instance by biogeochemical processes such as $CaCO_3$ dissolution and respiration.

Therefore, during high productive seasons, the primary production will increase TA and decrease DIC, while consuming CO_2 and nutrients (Xue and Cai, 2020). The uptake of NO_3^- will increase and the uptake of NH_4^+ will decrease TA in an ecosystem (Brewer and Goldman, 1976; Wolf-Gladrow et al., 2007). The production of 1 mol organic matter ($(CH_2O)_{106}(NH_3)_{16}H_3PO_4$) will generally increase TA by 17 mol TA (ΔTA_P) and decrease DIC by 106 mol and will change the TA and DIC concentrations (Chen, 1978). Therefore, ΔTA_P is used to calculate the expected amount of TA produced and decrease DIC by primary producers, according to the equation of ΔTA_{bio} from (Xue and Cai 2020), which was modified using the calculated ΔDIC_{excess}:

$$\Delta TA_P = -17/106 * \Delta DIC_{excess} \quad (8)$$

However, it is important to note, that the calculation of ΔTA_P is an overestimation assuming the measured TA is resulting only due to photosynthesis (NO_3^--fueled) or respiration. Additionally, the East Frisian WS is also influenced by tidal variability and other riverine inputs from land for instance Rhine River or Elbe River.

https://doi.org/10.5194/egusphere-2024-3048
Preprint. Discussion started: 23 October 2024

3 Results

3.1 Intertidal East Frisian Wadden Sea

3.1.1 Regional and seasonal variation

In July 2021, salinities were lowest on the route from Norddeich harbor to Norderney (25.21), and in the intertidal region around Norderney (Table 2; Fig. 2) in the Western WS. In summer 2022, the salinity on July 12 (31.16 - 32.03) increased by 2 - 3 salinity units compared to July 11 (28.28 - 29.43) in the Eastern WS (Table 2; Fig. 2). This indicates that during July 2022 cruise, there was a change in salinity range between the first and second leg of the cruise (in roughly the same region). A possible reason for these salinity differences could be the Neuharlingersiel sluice opening in the early morning of July 11, 2022, which could have influenced the salinity on this day. The turbidity in October 2021 showed a completely different pattern compared to all other seasons, with values from 96.08 – 306.46 NTU (Fig. 2), caused by rougher weather conditions during the campaign. However, slight regional differences in turbidity were measured, for instance in the Jade Bay in March 2022, as well as in the intertidal WS near Juist (Fig. 2).

Table 2: Overview of the different measured parameters: Temperature (°C), Salinity, pH, oxygen (% saturation), AOU (µmol L^{-1}), Chlorophyll a (Chl a in µg L^{-1}), $pCO_{2\ obs}$ (µatm) and Aragonite saturation Ωcal of all seasonal samplings. The given values of the Calcite saturation state (Ωcal) are separated in the low saline Ems Estuary and the East Frisian Wadden Sea (Eastern WS, Western WS) in high salinity waters.

Parameter	July 2021	October 2021	March 2022	May 2022	July 2022
Temperature (°C)	18.59 – 23.15*[1]	12.66– 16.57*[1]	3.89 – 6.47*[2]	9.65 – 18.19*[2]	17.36 – 21.88*[2]
Salinity	25.21 – 32.33*[1]	25.21 – 31.32*[1]	0.25 – 31.97*[2]	0.36 – 32.28*[2]	1.35 – 32.04*[2]
pH	7.71 – 8.16*[1]	7.64 – 8.13*[1]	7.33 – 8.13*[2]	7.25 – 8.56*[2]	7.30 – 8.08*[2]
Oxygen (% sat)					
East Frisian					
Wadden Sea:	109.7 ± 9.5*[1]	100.9 ± 5.3*[1]	104.9 ± 3.3*[1]	129.6 ± 15.3*[1]	101.2 ± 5.9*[1]
Ems Estuary:	–	–	77.8 ± 10.6	45.5 ± 20.8	65.6 ± 25.4
AOU (µmol L^{-1})					
East Frisian					
Wadden Sea:	-22.7 ± 22.2*[1]	-2.3 ± 14.4*[1]	-15.9 ± 10.9*[1]	-39.1 ± 97.2*[1]	-2.9 ± 14.2*[1]
Ems Estuary:	–	–	85.2 ± 41.3	164.2 ± 64.2	91.6 ± 70.2
Chl a (µg L^{-1})	25.6 ± 12.9*[1]	16.9 ± 8.9*[1]	13.3 ± 6.3*[2]	42.0 ± 27.9*[2]	23.2 ± 19.3*[2]
$pCO_{2\ obs}$ (µatm)					
East Frisian					
Wadden Sea:	–	521.6 ± 72.2*[1]	485.6 ± 73.2*[1]	319.4 ± 202.9*[1]	536.0 ± 116.5*[1]
Ems Estuary:	–	–	2306.9 ± 534.1	1521.5 ± 1318.4	2237.9 ± 1109.1
Ωcal					
East Frisian					
Wadden Sea:	3.8 ± 0.9*[1]	3.21 ± 0.6*[1]	2.6 ± 0.3*[1]	5.2 ± 1.1*[1]	3.8 ± 0.4*[1]
Ems Estuary:	–	–	0.9 ± 0.6	1.1 ± 0.7	1.9 ± 0.8

*[1] Cruises, containing the Western and Eastern part of the East Frisian Wadden Sea (Western WS & Eastern WS)
*[2] Cruises, which covered not only the intertidal regions, but also the Ems River Estuary

https://doi.org/10.5194/egusphere-2024-3048
Preprint. Discussion started: 23 October 2024

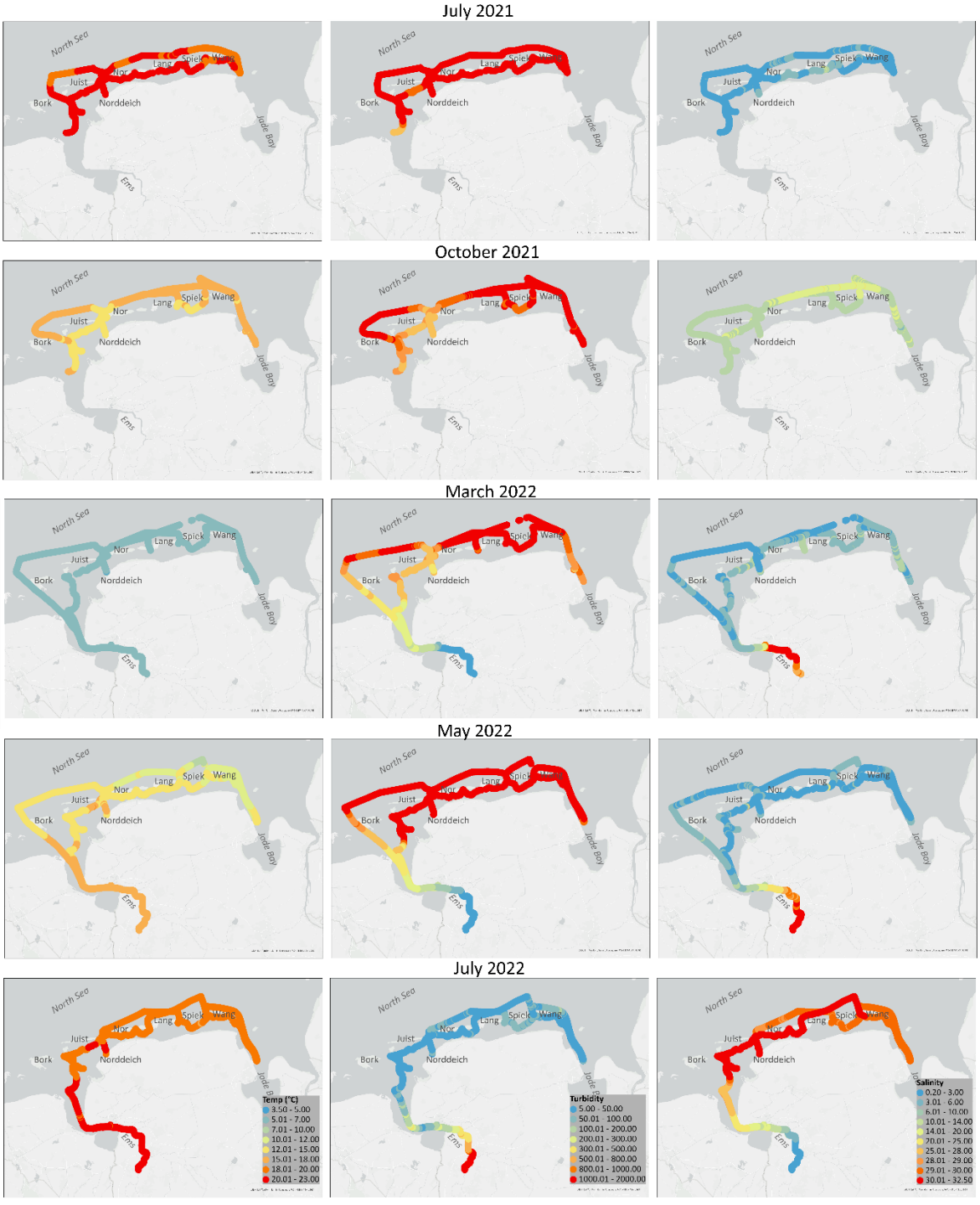

Figure 2: Results of all seasonal cruises from July 2021, October 2021, March 2022, May 2022 and July 2022 measured with the FerryBox. Temperature (°C), Salinity (PSU) and Turbidity (FNU). The map in this Figure was generated using ArcGIS. Data sources: LGLN, Esri, TomTom, Garmin, Foursquare, FAO, METI/NASA, USGS. © 2024 Julia Meyer.

https://doi.org/10.5194/egusphere-2024-3048
Preprint. Discussion started: 23 October 2024

A land to sea gradient was observed in pH in October 2021 (Fig. 3), which varied from 7.64 to 8.13 (Table 2). Higher values were measured in the North Sea regions (behind Juist, Norderney, Langeoog), whereas the lower values were measured closer to the mainland. The highest pH values were measured in May 2022 (Fig. 3; Table 2) with the highest variability and pH > 8 in the Western region, in front of Norderney. Regional differences with maximum pH values of > 8 in the higher salinity intertidal waters were measured during all seasons (Fig. 3).

The chlorophyll a in May 2022 was the highest (Table 2; Fig. 3) overall, with the greatest variance (Table 2), and especially, in the Western part of the East Frisian WS from Norderney to Borkum (up to 151.7 µg L^{-1}) (Fig. 3). In July 2021, the highest chlorophyll a measurements (up to 74.7 µg L^{-1}) were detected in the intertidal region from Norderney to Spiekeroog (Table 2; Fig. 3), whereas lower values (down to 2.8 µg L^{-1}) were observed in the North Sea regions of the transects. A similar pattern can be seen for July 2022 in the intertidal zone (Fig. 3), however no measurements of the transect from Norderney to Spiekeroog is available for chlorophyll a. This is also the case for October 2021 within the intertidal zone transects from Norderney to Wangeoog (Fig. 3).

A similar seasonal variability was observed for the oxygen (Table 2; Fig. 3). In July 2021 the measured oxygen ranged from 72.4 – 112.01 in % saturation (Fig. 3), with the highest values in the intertidal area of Langeoog. The oxygen saturation decreased from July 2021 to October 2021, on average by 8.8 ± 10.9 % saturation (Table 2; Fig. 3). The lowest oxygen saturation was measured on the transect from Norddeich to Norderney in October (down to ~ 57 % saturation). Until May 2022, oxygen saturation increased continuously over the year. The highest oxygen saturation (up to ~ 180 %) was measured in May 2022 in the intertidal region of Norderney in the Western WS and around Wangeoog in the Eastern WS (up to ~ 152 %) (Table 2; Fig. 3). However, saturations below 100 % were measured in the section from Norddeich harbor to Norderney (down to 84 % saturation) (Fig. 3). Overall, oxygen saturation in the East Frisian WS decreased by a mean value of 28.4 ± 16.4 % from May 2022 to July 2022 (Fig. 3), resulting in slightly lower oxygen saturation in July 2022 compared to the year before (Table 2). The opposite picture was also observed for AOU (not shown), with negative values as it became more saturated (> 100 % saturation) (Table 2). The observed pCO_2 ($pCO_{2\ obs}$) was highest in July 2022 and lowest in May 2022 (down to 141.3 µatm) in the intertidal zone of the Western WS. The average decrease in $pCO_{2\ obs}$ was 166.2 ± 276.1 µatm from March 2022 to May 2022 (Table 2; Fig. 4) (see also section 3.1.2).

https://doi.org/10.5194/egusphere-2024-3048
Preprint. Discussion started: 23 October 2024

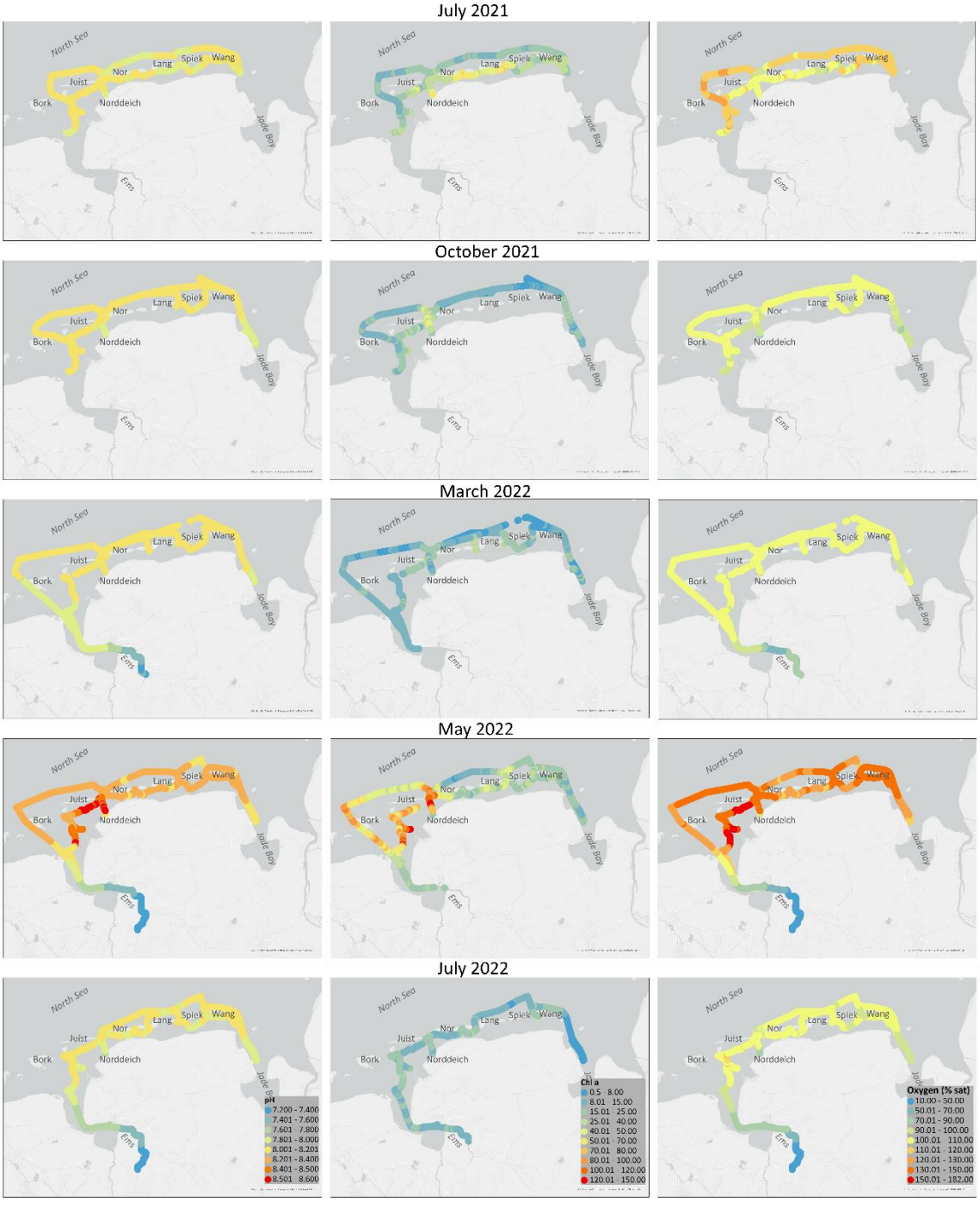

Figure 3: Results of all seasonal cruises from July 2021, October 2021, March 2022, May 2022 and July 2022 measured with the FerryBox. pH, Chlorophyll a (Chl a in µg L^{-1}) and oxygen (% saturation). The map in this Figure was generated using ArcGIS. Data sources: LGLN, Esri, TomTom, Garmin, Foursquare, FAO, METI/NASA, USGS. © 2024 Julia Meyer.

https://doi.org/10.5194/egusphere-2024-3048
Preprint. Discussion started: 23 October 2024

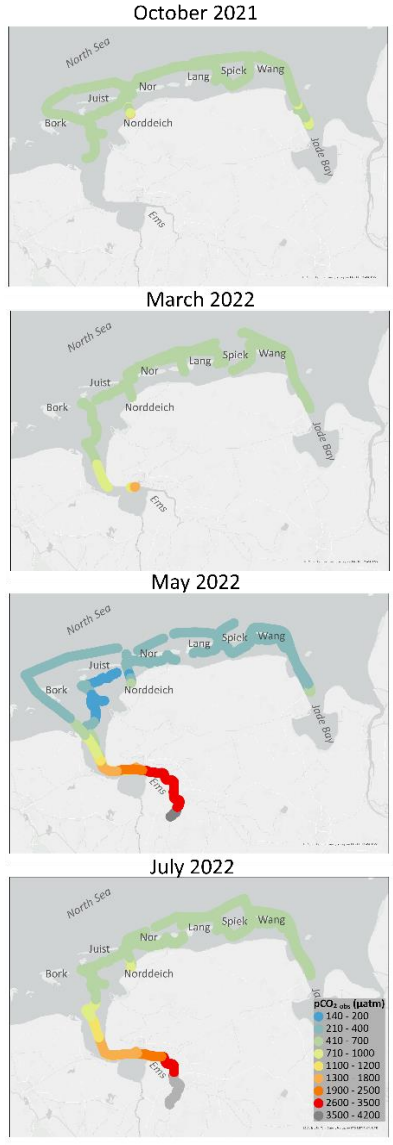

240

Figure 4: $pCO_{2\ obs}$ (µatm) of October 2021, March 2022, May 2022 and July 2022 measured with the FerryBox. The map in this Figure was generated using ArcGIS. Data sources: LGLN, Esri, TomTom, Garmin, Foursquare, FAO, METI/NASA, USGS. © 2024 Julia Meyer.

https://doi.org/10.5194/egusphere-2024-3048
Preprint. Discussion started: 23 October 2024

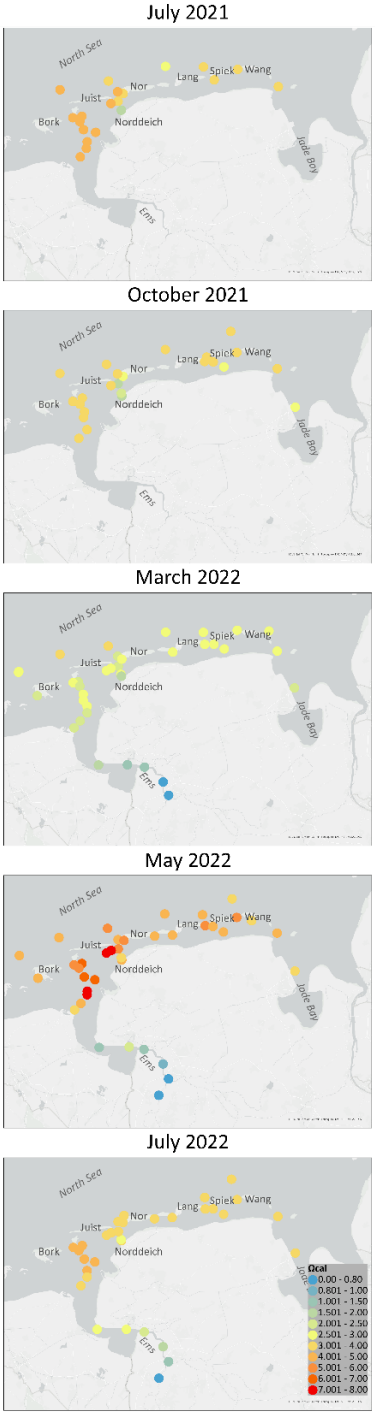

245 **Figure 5: Calculated Ωcal saturation of the seasonal cruises. July 2021, October 2021, March 2022, May 2022 and July 2022. The map in this Figure was generated using ArcGIS. Data sources: LGLN, Esri, TomTom, Garmin, Foursquare, FAO, METI/NASA, USGS. © 2024 Julia Meyer.**

https://doi.org/10.5194/egusphere-2024-3048
Preprint. Discussion started: 23 October 2024

The calcite saturation (Ωcal) was calculated (Lewis et al., 1998; Weiss, 1974) for all seasonal cruises to observe where $CaCO_3$ dissolution and formation may occurs seasonally. During all seasons, Ωcal was supersaturated in the intertidal East Frisian WS, ranging from 1.5 – 7.5 (Table 2), but with a pronounced seasonal pattern. Low values (< 2.0) were mainly calculated in October 2021 and March 2022 (Table 2; Fig. 5). Higher, oversaturated Ωcal values (> 2.5) were observed during more productive seasons (July 2021, July 2022, May 2022). However, the highest variability of Ωcal was found in May 2022 with values > 1 in 80 % of the stations and reaching up to 7.52 in the intertidal region of Juist and Borkum (Table 2; Fig. 5). In contrast, in the Ems River estuary, Ωcal saturation decreased (down to < 1) with decreasing salinity during all seasons and was the lowest in March 2022 (Table 2; Fig. 5). In summer (July 2021, July 2022), a decrease of Ωcal in the East Frisian WS from West to East can be observed, regionally (Fig. 5). The high Ωcal saturation (up to 7.5) in May 2022 in the intertidal zone near Juist and Borkum is outstanding (Fig. 5). These high and oversaturated values can support $CaCO_3$ formation in this region, and thus calcification of organisms during this highly productive season (May 2022).

3.1 2 Seasonal Shifts in the Dominance of Biological and Thermal Components of pCO_2

The thermal effect was removed from $pCO_{2\ obs}$ measurements (Fig. 4) to isolate the portion of pCO_2 that can be explained by biological effects ($pCO_{2\ bio}$). The remaining $pCO_{2\ bio}$ reflects the biologically influenced pCO_2, including the effects of biological production and consumption of CO_2, ocean mixing processes, and freshwater inputs(Chierici et al., 2006; Lüger et al., 2004; Tozawa et al., 2022).

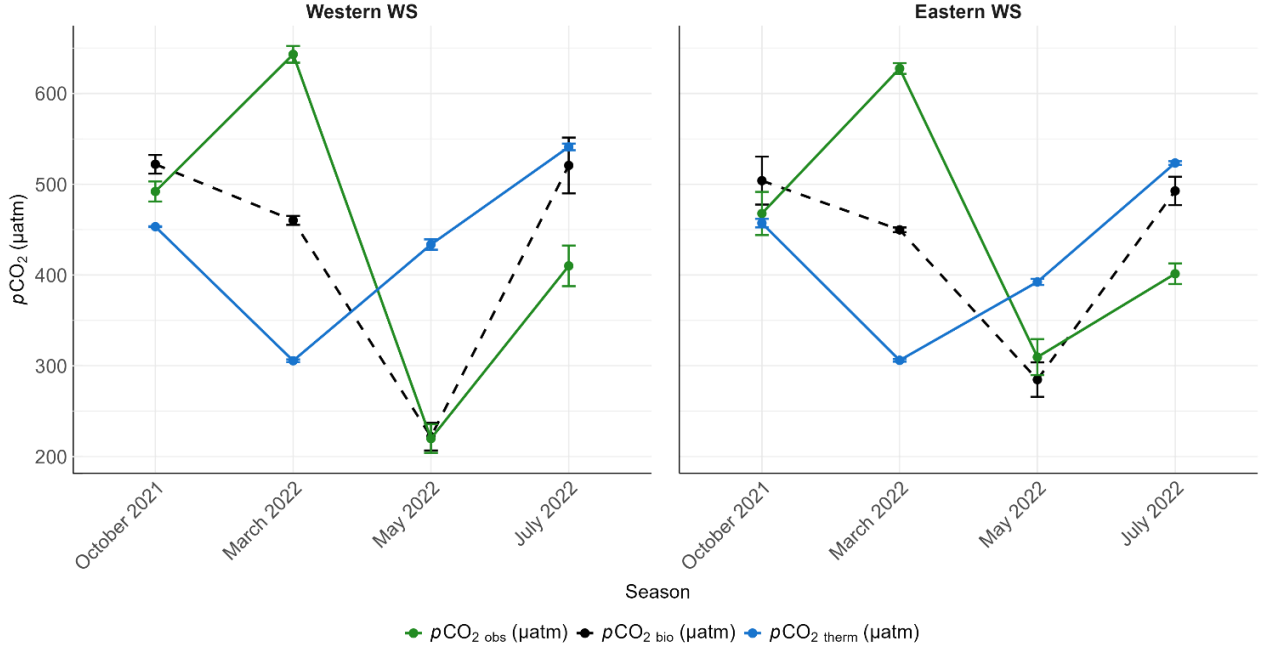

Figure 6: Seasonal thermal component, $pCO_{2\ therm}$, biological component, $pCO_{2\ bio}$ and pCO_2 observations, $pCO_{2\ obs}$ mean values with the related error bars in the Western and Eastern WS.

https://doi.org/10.5194/egusphere-2024-3048
Preprint. Discussion started: 23 October 2024

The seasonal variability of $pCO_{2\ obs}$, $pCO_{2\ therm}$ and $pCO_{2\ bio}$ are illustrated in Figure 6. The $pCO_{2\ therm}$ (453.2 µatm) was slightly lower compared to $pCO_{2\ bio}$ (492.0 µatm) in October 2021 (Fig. 6), in the Western WS. In March 2022, the biological influence was higher (643.1 µatm) in the Western WS, compared to the $pCO_{2\ therm}$ indicating both thermal and biological effects influencing the $pCO_{2\ obs}$ (Fig. 6). By May 2022 the pattern shifted, with substantial low $pCO_{2\ bio}$ (219.9 µatm), while $pCO_{2\ therm}$ remained relatively high (433.6 µatm). This predominance of the biological over the thermal component during May contributed to the overall drawdown of $pCO_{2\ obs}$ (Fig. 6), with similar errors of 15.7 µatm for $pCO_{2\ bio}$ and 15.2 µatm for $pCO_{2\ obs}$. Finally, from May 2022 to July 2022, all pCO_2 components increased, with the thermal influence surpassing the biological component. This implies higher thermal influence than biological in the Western WS (Fig. 6).

The Eastern WS exhibits a similar pattern in $pCO_{2\ obs}$, $pCO_{2\ therm}$ and $pCO_{2\ bio}$ with slightly lower values across all seasons compared the Western WS (Fig. 6). The results demonstrate a clear seasonal shift in the dominance of biological and thermal influences on pCO_2. During the colder months (October 2021, March 2022), thermal processes had a more notable impact on $pCO_{2\ obs}$. In contrast, biological processes played a more substantial role during the warmer months (May 2022, July 2022), particularly in May, when the biological influence was most pronounced in both regions (Fig. 6).

3.1.3 TA and DIC Variability

Large variability in DIC and TA was observed in the East Frisian WS, seasonally but also regionally along the land to sea gradient (Table 3; Fig. 7). Higher TA were measured in the intertidal region in summer (July 2021, July 2022) (Fig. 7). In July 2021, TA ranged from ~ 2273 µmol kg^{-1} in the Jade Bay (Eastern WS) and increased regionally westward (up to ~ 2465 µmol kg^{-1}) to Norderney (Table 3; Fig. 7). Figure 8 also shows the higher measured TA in summer (July 2021, July 2022) in the intertidal region compared to the other seasons. In July 2021, all measured TA values are above or slightly below the mixing line with a negative slope (- 24.9 µmol kg^{-1} per salinity unit) in the intertidal zone of the East Frisian WS (Fig. 8a), indicating TA production in this region. In July 2022, lower TA values were measured during the first leg of the cruise when salinities were lower (28 - 29) (Table 3; Fig. 7; Fig. 8a), but a similar slope (- 23.3 µmol kg^{-1} per salinity unit) of the short mixing line in Figure 8a was observed. During the July 2022 cruise, when higher salinities were measured (up to 32), the TA values were similar to those of July 2021, with a negative slope of - 25.1 µmol kg^{-1} per salinity unit, slightly above the mixing line, indicating TA production in the intertidal zone (Fig. 8a). The DIC concentrations also showed a similar pattern during both summer cruises (Table 3; Fig. 8b), with a negative slope of - 49.0 µmol kg^{-1} per salinity unit in July 2021 and in July 2022 in the Eastern WS of - 44.3 µmol kg^{-1} per salinity unit (Fig. 8b).

In October 2021, the highest TA concentrations were measured at a station near Norddeich (2571 µmol kg^{-1}) in the Western WS (Fig. 7). DIC shows a very similar pattern as for TA during this season (Fig. 7). The DIC values reached a maximum of 2516 µmol kg^{-1} in the intertidal zone in front of Norderney and decreased with increasing longitude to a minimum of 2158 µmol kg^{-1} (Fig. 7). The mixing plot of TA in October 2021 shows a negative mixing line in the Western WS (- 25.4 µmol kg^{-1} per salinity unit), whereas the Eastern WS shows an almost linear mixing line with a positive slope of 13.1 µmol kg^{-1} per salinity unit (Fig. 7; Fig. 8c).The DIC mixing plot (Fig. 8d) shows a similar picture in the Western WS to TA, with a

https://doi.org/10.5194/egusphere-2024-3048
Preprint. Discussion started: 23 October 2024

300 negative slope (- 46.9 mol kg^{-1} per salinity unit). In March 2022, lower DIC concentrations (< 2200 µmol kg^{-1}) were measured further offshore behind the islands of Borkum, Juist and Norderney and these increased slightly closer to land (Fig. 7). A few stations in the intertidal zone also recorded higher concentrations than others in the surrounding area. Little variation of TA and DIC in the intertidal zone was found, resulting in an almost linear mixing line of TA and DIC within this region (Fig. 8e, f) in March 2022.

305 **Table 3: Overview of different the parameters TA (µmol kg^{-1}), DIC (µmol kg^{-1}) and [TA-DIC] (µmol kg^{-1}) of all seasonal samplings in average with the standard deviation.**

Parameter	July 2021	October 2021	March 2022	May 2022	July 2022
TA (µmol kg^{-1})					
Western WS:	2403.4 ± 27.4	2406.7 ± 53.6	2358.6 ± 27.8	2378.9 ± 39.0	2380.2 ± 42.7
Eastern WS:	2283.5 ± 10.2	2367.8 ± 5.3	2347.2 ± 11.8	2349.7 ± 9.8	2337.2 ± 35.2
Ems Estuary:	–	–	2609.2 ± 68.0	2741.3 ± 77.4	2697.7 ± 101.1
DIC (µmol kg^{-1})					
Western WS:	2185.8 ± 48.2	2257.1 ± 91.0	2237.7 ± 37.8	2065.5 ± 107.0	2184.4 ± 43.3
Eastern WS:	2124.1 ± 10.3	2182.8 ± 18.2	2211.8 ± 11.8	2089.2 ± 38.0	2142.3 ± 27.6
Ems Estuary:	–	–	2681.3 ± 124.4	2791.5 ± 136.0	2682.6 ± 169.1
[TA–DIC] (µmol kg^{-1})					
Western WS:	217.55 ± 51.9	150.5 ± 47.1	120.9 ± 30.2	313.3 ± 76.1	196.8 ± 26.7
Eastern WS:	159.44 ± 16.4	184.9 ± 19.9	137.9 ± 11.0	260.5 ± 34.7	194.9 ± 21.1
Ems Estuary:	–	–	-72.1 ± 70.7	-50.2 ± 77.6	15.1 ± 69.2

The mean measured TA in the Western WS in May 2022 was 2378.9 µmol kg^{-1} in the intertidal zone (Table 3, Fig. 7), indicating a slight increase in TA from March to May 2022. Most of the TA in the intertidal zone are close to or above the
310 mixing line, with similar negative slopes in the Western WS (- 15.6 µmol kg^{-1} per salinity unit) and in the Eastern WS (- 15.3 µmol kg^{-1} per salinity unit) (Fig. 8g). The lowest DIC values (down to 1872 µmol kg^{-1}) in this study were also measured in the intertidal zone of the Western WS in spring (Table 3; Fig. 7; Fig. 8h). The DIC concentration in May 2022 was the lowest overall measured in this study, which is why the DIC values are below the mixing line (Fig. 8h).

During all seasons, the TA concentration was higher than the measured DIC concentration, which can be seen in the positive
315 values of [TA-DIC] (Table 3). The highest positive [TA-DIC] was calculated in May 2022, followed by the summer seasons (July 2021, July 2022), October 2021 and March 2022. The lowest [TA-DIC] was calculated in March 2022 and October 2021 (Table 3). The three lowest [TA-DIC] values in October 2021, March 2022 and July 2021 were the stations, which are located next to the harbour Norddeich. As described above, these showed already differences to the other stations in the parameters of the FerryBox (Fig. 2; Fig. 3; Fig. 4).

https://doi.org/10.5194/egusphere-2024-3048
Preprint. Discussion started: 23 October 2024

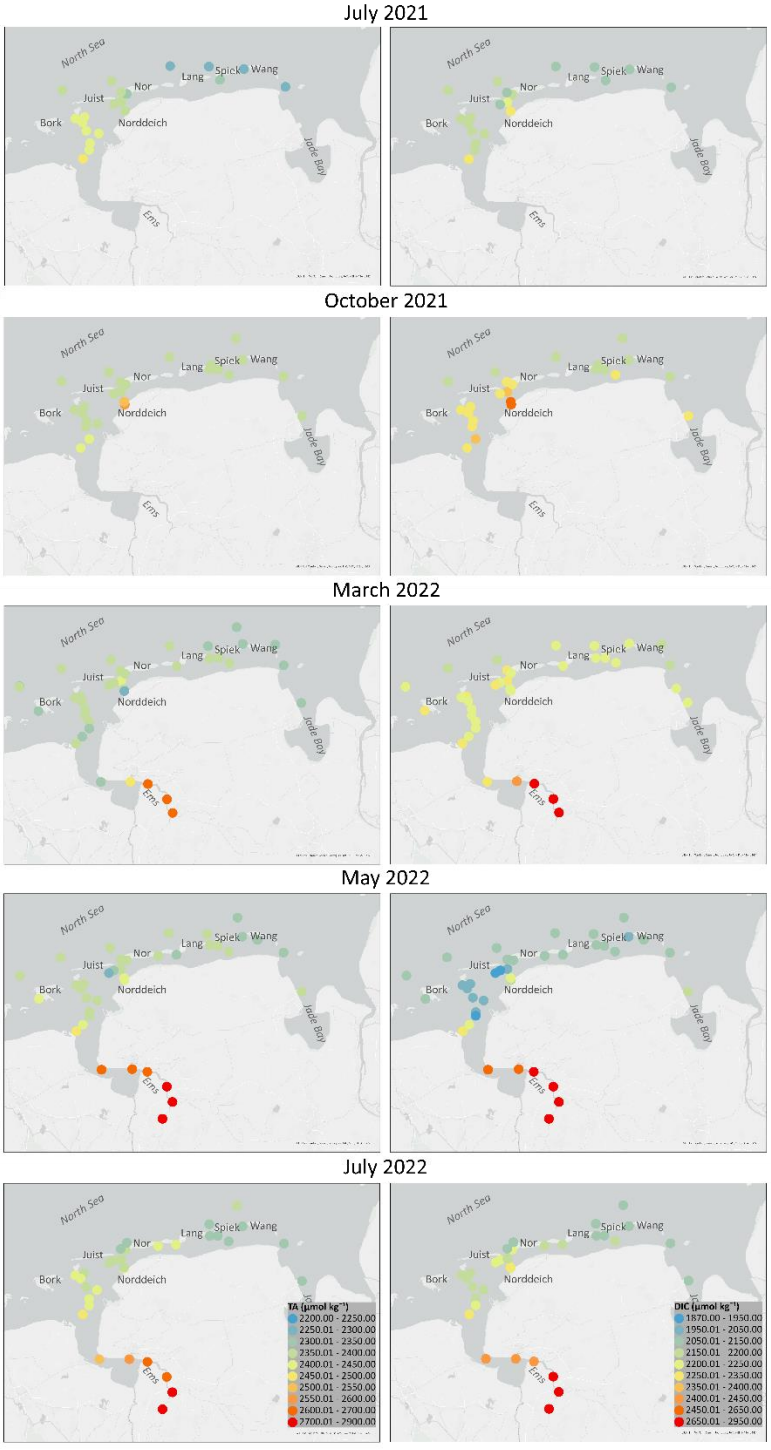

Figure 7: Measured results of TA and DIC of all seasonal cruises of July 2021, October 2021, March 2022, May 2022 and July 2022. All TA and DIC values are in µmol kg $^{-1}$). The map in this Figure was generated using ArcGIS. Data sources: LGLN, Esri, TomTom, Garmin, Foursquare, FAO, METI/NASA, USGS. © 2024 Julia Meyer.

https://doi.org/10.5194/egusphere-2024-3048
Preprint. Discussion started: 23 October 2024

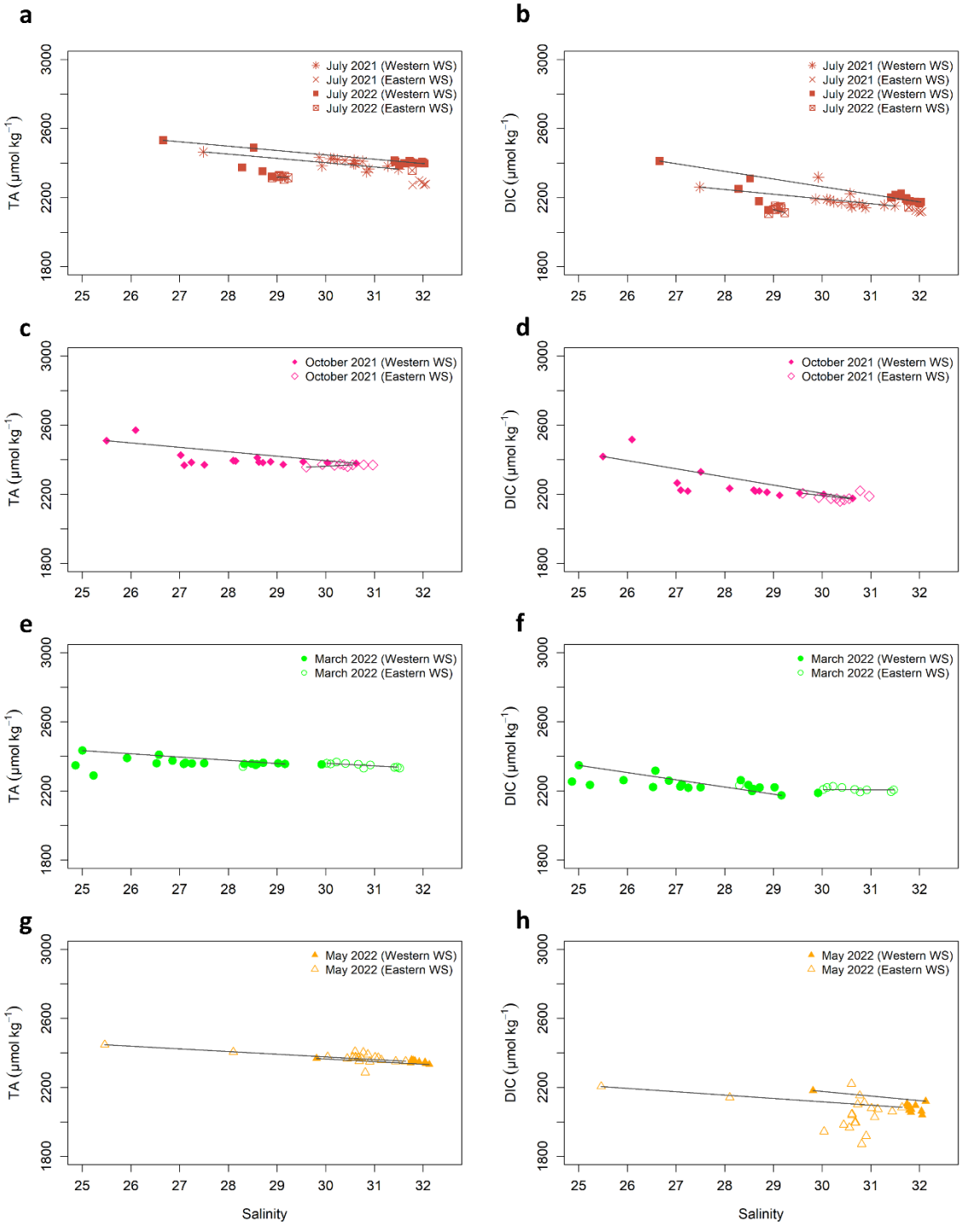

325 **Figure 8: TA (µmol kg^{-1}) and DIC (µmol kg^{-1}) mixing plots, against salinity of July 2021 (a, b), October 2021 (c, d), March 2022 (e, f), May 2022 and July 2022 (a, b) at > 25 salinity, separated by the different regions (Eastern WS, Western WS) of the studied intertidal East Frisian WS.**

https://doi.org/10.5194/egusphere-2024-3048
Preprint. Discussion started: 23 October 2024

3.2 Regional and seasonal variation of the Ems River Estuary

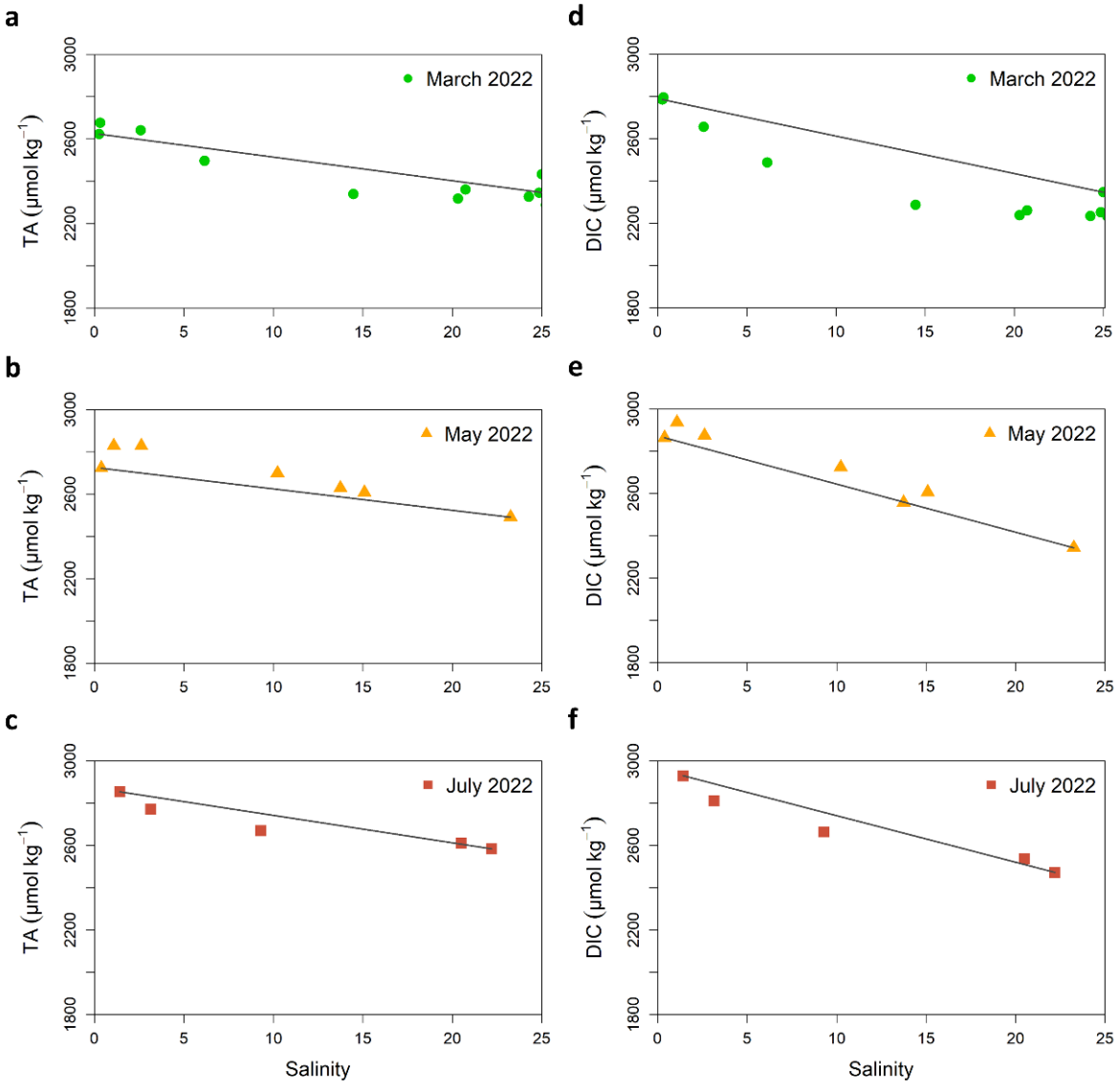

330 **Figure 9: TA (µmol kg^{-1}) and DIC (µmol kg^{-1}) mixing plots, against salinity of July 2021 (a, b), October 2021 (c, d), March 2022 (e, f), May 2022 and July 2022 (a, b) at > 25 salinity, separated by the different regions (Eastern WS, Western WS) of the studied intertidal East Frisian WS.**

Within the Ems River Estuary the temperature was lowest in March 2022 (down to ~5 °C) and highest (up to 21.9 °C) in July 2022 (Table 2; Fig. 2). The turbidity in the Ems River estuary increased with lower salinity during all seasons, with decreasing
335 pH (down to 7.33) (Fig. 3). The chlorophyll a was relatively low to the intertidal WS in March 2022 (down to ~ 9 µg L^{-1}) and in July 2022 (down to 11.9 µg L^{-1}) (Table 2; Fig. 3). Chlorophyll a was higher in May 2022 (up to 25.1 µg L $^{-1}$) than in other

https://doi.org/10.5194/egusphere-2024-3048
Preprint. Discussion started: 23 October 2024

periods in the Ems River estuary at the lowest salinity level (17.60) where chlorophyll a was measured (Table 2; Fig. 3). Overall, the oxygen saturation was also lower in the Ems River estuary compared to the intertidal WS, down to 62.8 %sat in March 2022 (Fig. 3). Oxygen saturation decreased further with decreasing salinity in May 2022 and July 2022 to 20.2 %sat and 13.44 %sat respectively (Fig. 3). The $pCO_{2\ obs}$ concentration showed the vice vera picture of oxygen saturation, which increased with decreasing salinity (Fig. 4). The $pCO_{2\ obs}$ was observed from March 2022 to May 2022 in the Ems River estuary, with values reaching 2307 ± 534 µatm in March and 1522 ± 1318 µatm in May. The calculated difference between these values is 785 ± 1421 µatm, indicating significant variability (Fig. 4).

The Ωcal dropped with decreasing salinity in the Ems River estuary and remained undersaturated (> ~ 0.8) during all seasons, leading to shells and skeletons made of $CaCO_3$ to become vulnerable to dissolution (Table 2; Fig. 5). In the Ems River estuary, the measured TA and DIC increased with lower salinity during all seasons (Fig. 7; Fig. 9). Maximum TA values of 2676 µmol kg^{-1} were recorded in the Ems River estuary in March 2022, while values in the intertidal zone were lower (Table 2; Fig. 7; Fig. 9). However, [TA–DIC] cannot be used at low salinity (e.g. <20) and when [TA–DIC] is < ~50 µmol kg^{-1}, where the relationships of [TA–DIC] with pH and/or ocean acidification are nonlinear, these low values also occur in oxygen minimum zones (Xue and Cai 2020). This is the reason, why we only are showing the results of the intertidal region of the East Frisian WS (Western WS, Eastern WS) (Table 3, Fig. 14, Fig. 15).

The Ems River estuary shows highest NO_3^- concentrations in March 2022 (up to 341.47 µmol L^{-1}), decreasing also in summer (down to 97.50 µmol L^{-1}) (Fig. 12), yet remains also high. In contrast, NH_4^+ was also high in in the Ems River estuary in March 2022, however it dropped constantly from 19.73 µmol L^{-1} down to the detection limits > 0.01 µmol L^{-1}. NO_2^- concentrations also dropped from March 2022 to May 2022 (Fig. 12).

3.3 Regional Variability and Seasonal Trends in ΔDIC_{excess} and ΔTA_{excess} in the Wadden Sea

Higher fluctuations in the Western WS in comparison to the Eastern WS were observed in ΔDIC_{excess} and ΔTA_{excess} (Fig. 10), seasonally and regionally. In the Western WS ΔDIC_{excess} values were mostly positive in July 2021, October 2021 and in July 2022, indicating production of DIC (Fig. 10). This was also observed in other parameters described before and in the mixing plots of TA and DIC with salinity (Fig. 8). The mean ΔDIC_{excess} for the Western WS in March 2022 (-14.2 ± 51.5 µmol kg^{-1}) shows more stations consuming than producing DIC (Fig. 10). This pattern of DIC, with stations above and below the mixing line, is also shown in Fig. 8f. The greatest variability of ΔDIC_{excess} is observed in May 2022 (- 60.9 ± 84.4 µmol kg^{-1}) in the Western WS with some outlying values next to the Norddeich harbor above zero (Fig. 8; Fig. 10). If we treat the two stations near the port of Norddeich as outliers in July 2022, which are strongly negative in Fig. 10, we obtain positive mean values for ΔDIC_{excess} (11.9 ± 18.7 µmol kg^{-1}) in the WS, which means that production exceeds consumption of DIC. This was not very clear in the mixing plot shown in Fig. 8b, however.

https://doi.org/10.5194/egusphere-2024-3048
Preprint. Discussion started: 23 October 2024

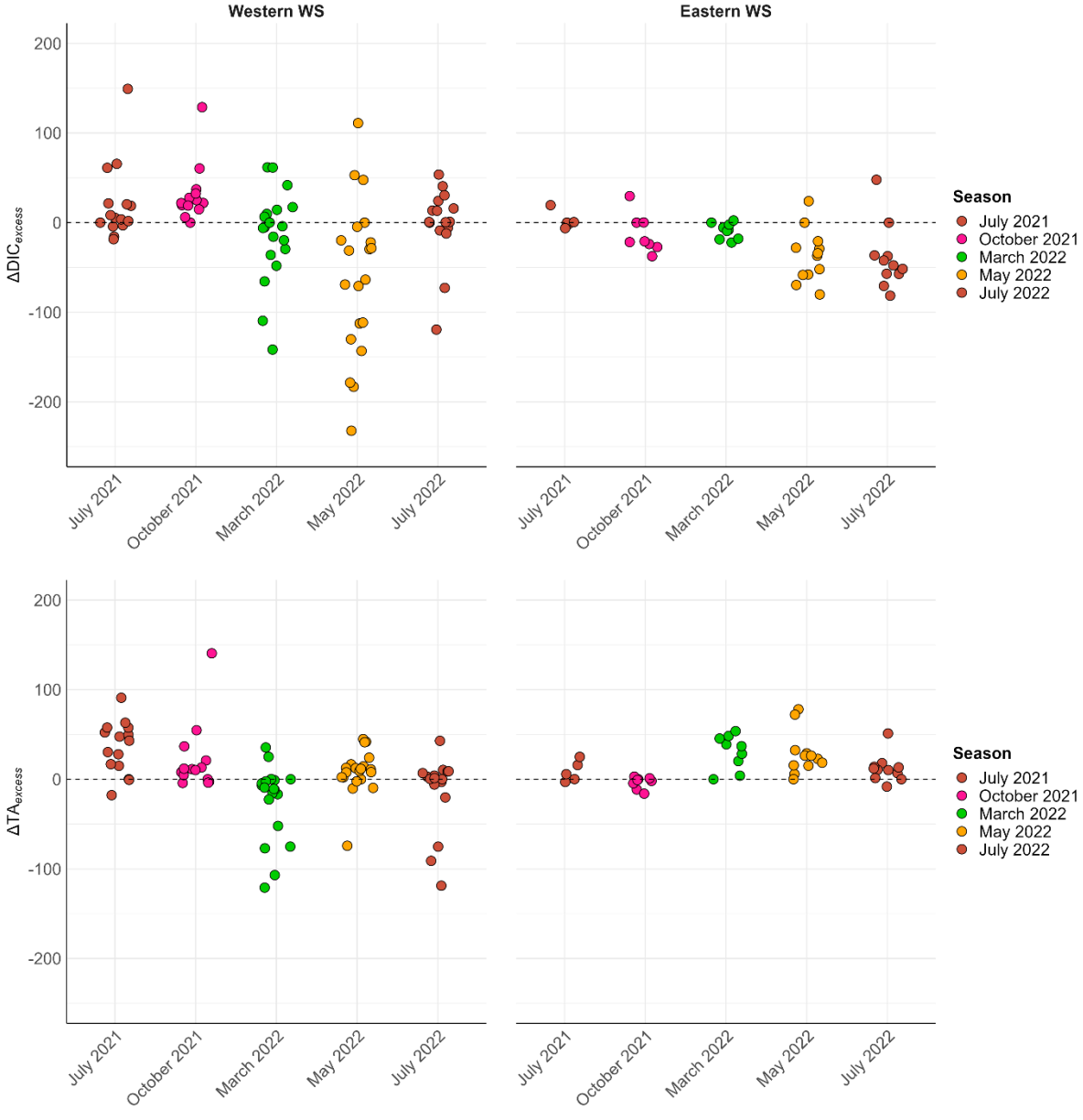

Figure 10: Calculated ΔDIC_{excess} and ΔTA_{excess} values of all seasons in on the Eastern WS and Western WS in µmol kg^{-1}of each season.

370 Excluding the strongly negative values of ΔTA_{excess} (Fig. 10) and treating them as outliers in July 2022 in the Western WS, we obtain a positive mean of 4.5 ± 13.5, indicating production, as evident in Fig. 8a. In contrast, higher mean value of ΔTA_{excess} (35.6 ± 27.9 µmol kg^{-1}) in July 2021 implies a higher production in TA (Fig. 8a; Fig. 10) in the Western WS. The ΔTA_{excess} values in October 2021 are mostly close to zero, except for the stations close to land (Norddeich). If we exclude these stations,

https://doi.org/10.5194/egusphere-2024-3048
Preprint. Discussion started: 23 October 2024

the mean ΔTA_{excess} value of 12.4 ± 16.3µmol kg-^{1}, indicating slight production of TA (Fig. 10). This finding, however, is inconsistent with the mixing plots (Fig. 8c), suggesting that mixing effects between the Ems River estuary and the intertidal Western WS may be contributing to the observed changes in TA (Fig. 8c). In March 2022, negative ΔTA_{excess} values were measured near the Ems River estuary, suggesting consumption of TA in this region. However, positive values (ranging from ~ 10 – 50 µmol kg^{-1}) in the intertidal region around Juist and Norderney indicate production of TA. Despite these observations, the mixing plot does not show a clear pattern of TA production and consumption (Fig. 8e), indicating a mixing effect of riverine water masses coming from the Ems River estuary (Fig. 10). In May 2022, the ΔTA_{excess} values suggest a slight production of TA. Almost all values, except for one strongly negative station located near Juist, are positive, resulting in a mean value of 8.2 ± 8.7 µmol kg^{-1} (Fig. 10). This slight positive trend is also visible in Fig. 8g, where most points are positioned just above or on the mixing line.

The Eastern WS exhibits lower variability in ΔDIC_{excess} and ΔTA_{excess}. In October 2021 and March 2022, ΔDIC_{excess} values were close to zero, with mean values of 2.5 ± 10.4 µmol kg^{-1} and - 9. ± 8.3 µmol kg^{-1}, respectively (Fig. 10). This pattern suggests a slight production of DIC in October 2021 and consumption in March 2022 (Fig. 8f), however, this was not clearly evident in the mixing plots shown in Fig. 8, which may be due to higher riverine influence. In May 2022, predominantly negative ΔDIC_{excess} values were observed, with a mean value of - 36.9 ± 28.2 µmol kg^{-1} (Fig. 10). This pattern is likely attributable to photosynthesis, which is especially pronounced in spring. The lowest variability in ΔDIC_{excess} was observed in July 2021 with a mean value of 8.7 ± 10.6 µmol kg^{-1}, suggesting slight production of DIC, lower to the Western WS (Fig. 10). The ΔTA_{excess} shows a similar pattern in July 2021 (mean value of 8.7 ± 10.4 µmol kg^{-1}) and July 2022 (mean value of 11.7 ± 14.4 µmol kg^{-1}), both indicating a production of TA (Fig. 8; Fig. 10). Nevertheless, only a small number of stations were available for this calculation within the season, and only the Weser River was included in the Eastern WS, highlighting the importance of also considering other rivers like the Rhine and the Elbe. Additionally, the time periods of river sampling for the calculation of ΔDIC_{excess} and ΔTA_{excess} values did not always coincide exactly with the sampling times during the *RV Burchana* cruises. Such discrepancies could lead to deviations, meaning that the results can only indicate a general trend or seasonal pattern. This is also evident in the results from July 2022, where the ΔDIC_{excess} displays a different pattern compared to the Western WS. While a negative mean value of - 39.5 ± 34.1 µmol kg^{-1} ΔDIC_{excess} was calculated in the Eastern WS, positive ΔDIC_{excess} values (11.9 ± 18.7 µmol kg^{-1}) was determined in the Western WS (Fig. 10). It is important to note that on July 11, the Eastern WS was influenced by the opening of the sluice at Neuharlingersiel, which altered salinity during the sampling day and lower TA and DIC concentrations (Fig. 7; Fig. 8a, b; Fig. 10). As a result, the consumption of DIC and production of TA in the Eastern WS could partly be attributable to land-based inputs (Fig. 2; Fig. 8a, b; Fig. 10), decreasing the real signal of TA production and DIC consumption in this region.

3.4 Estimation of TA generation via primary production and nutrient dynamics

For ΔTA_P, greater variability is visible in the Western WS compared to the Eastern WS regionally (Fig. 11). At different times, there are both positive and negative deviations from the zero line, indicating periodic fluctuations in photosynthetic activity

https://doi.org/10.5194/egusphere-2024-3048
Preprint. Discussion started: 23 October 2024

with TA production and TA consumption due to other processes (e.g., respiration, $CaCO_3$ precipitation). While the values of ΔTA_P exhibit lower variability in July 2021 and October 2021, except for the stations near the Norddeich harbor, the other seasons show greater variability. Thus, a mean value of - 3.4 ± 6.6 µmol kg^{-1} in July 2021 and a mean value of - 5.1 ± 13.3 µmol kg^{-1} in October 2021 (excluding the stations near Norddeich) can be observed (Fig. 11). This indicates a lower effect from photosynthesis, suggesting that other biogeochemical processes contribute to TA production during these seasons (Fig. 11).

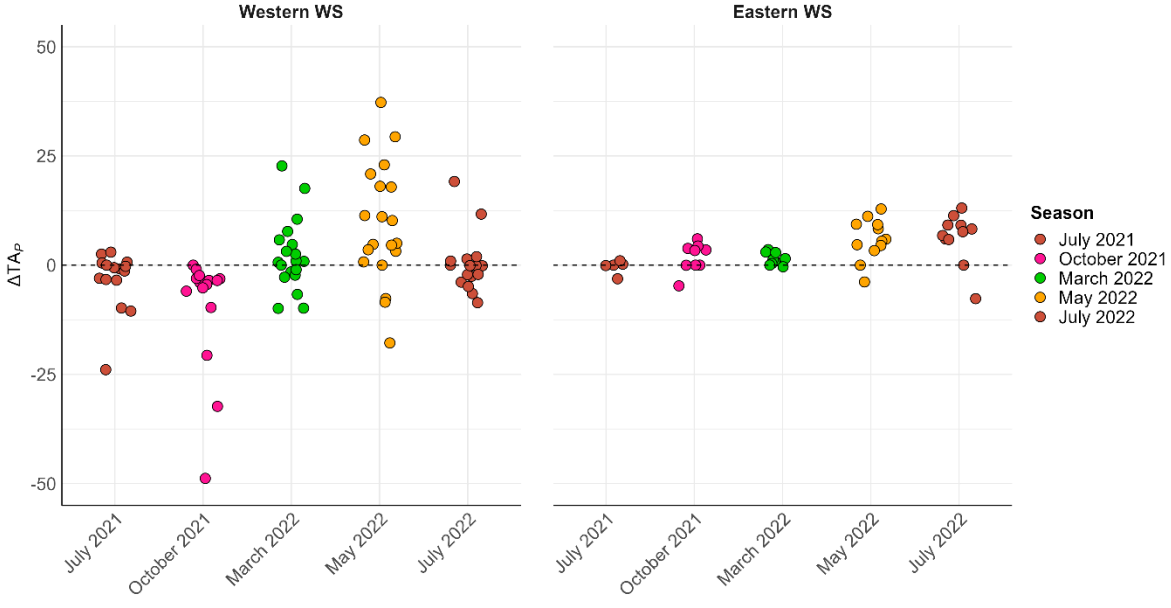

Figure 11: Calculated ΔTA_P values in µmol kg^{-1} of all seasons in the Western WS and Eastern WS.

In the Western WS, the mean value was 2.3 ± 8.0 µmol kg^{-1} in March 2022 and 9.8 ± 6.6 µmol kg^{-1} in May 2022. Therefore, March 2022 and May 2022 show a wide range of ΔTA_P values, with many data points above zero, indicating as higher tendency to biological productivity due to primary production, generating TA (Fig. 10) driven by decreasing NO_3^- concentrations from March to May 2022 (Fig. 11). Overall, approximately 80% of the sampled stations had positive ΔTA_P values ($\Delta TA_P > 0$) in May, indicating TA production can be explained by primary production (Fig. 11). In July 2022, the ΔTA_P values were more dispersed, with a mean value of 0.3 ± 6.5 µmol kg^{-1}. Around 40% of the stations had positive values, while approximately 60% of the values were negative in July 2022. This suggests that primary production and other biogeochemical processes contribute to the generation of TA in the Western WS (Fig. 10; Fig. 11).

The ΔTA_P values in the Eastern WS exhibit less variability compared to the Western WS. Most data points are clustered around zero across all seasons, indicating minimal changes in alkalinity. There are fewer stations and extreme values in the Eastern WS, suggesting more stable alkalinity production over the observed seasons. The highest variability of ΔTA_P in the Eastern WS was measured in May (5.9 ± 4.5 µmol kg^{-1}) and July 2022 (6.3 ± 5.5 µmol kg^{-1}). TA production is also visible here in May

https://doi.org/10.5194/egusphere-2024-3048
Preprint. Discussion started: 23 October 2024

2022, but not as pronounced as in the Western WS, where we encountered signals of higher biological productivity (Fig. 11). Once again, it is important to mention that the opening of the Neuharlingersiel sluice may possibly have influenced the values of ΔTA_P in July 2022 (Fig. 11).

A clear seasonal pattern can also be seen in the measured nutrients (Fig. 12). For NO_2^- and NH_4^+ a decrease in concentrations was observed from October 2021 to May 2022, except in the East part of the East Frisian WS for NO_2^- (Fig. 12), where the concentration did not change. NO_3^- concentration ranged seasonally, with an increasing trend from summer to March 2022 (up to 66.28 µmol L^{-1}) in the intertidal East Frisian WS. In May 2022, the NO_3^- concentrations decreased again below the detection limit of the instrument (> 0.01 µmol L^{-1}) at some stations, mainly in the Western part (Fig. 12). This analogous seasonal tendency possibly will point to common sources and sinks.

Overall, from March 2022 to May 2022 there was an average decrease in NO_3^- 19.29 ± 18.11 µmol kg^{-1} (Fig. 12; Fig. 13). TA slightly increased by 9.1 ± 29.2 µmol kg^{-1} (Fig. 7; Fig. 8; Fig. 10; Fig. 11), while DIC decreased on average by 159.4 ± 125.4 µmol kg^{-1} (Fig. 7; Fig. 8; Fig. 10). The differences of NO_3^- and SiO_2 for all stations between March and May 2022 (ΔNO_3^-, ΔSiO_2) were plotted against the DIC difference between March and May (ΔDIC, Fig. 13). For ΔNO_3^- a regression line was fitted with equation of y = 6.90x + 29.089 (R^2 = 0.4637, *p*- value = < 0.05, Fig. 13), while the ΔSiO_2 regression has an equation of y = 8.11x + 50.605 (R^2 = 0.2165, *p*- value = < 0.05, Fig. 13). The slope of both regression lines is close to the Redfield Ratio (Redfield 1963) of 106/16 = 6.625 for NO_3^- (6.90, Fig. 13) and 106/15 = 7.067 for SiO_2 (8.11, Fig. 13), indicating that the identified enhanced primary production in this region in the spring, along with nutrient uptake of the available inorganic nutrient species most likely lead to a concomitant decrease in DIC (Fig. 13).

https://doi.org/10.5194/egusphere-2024-3048
Preprint. Discussion started: 23 October 2024

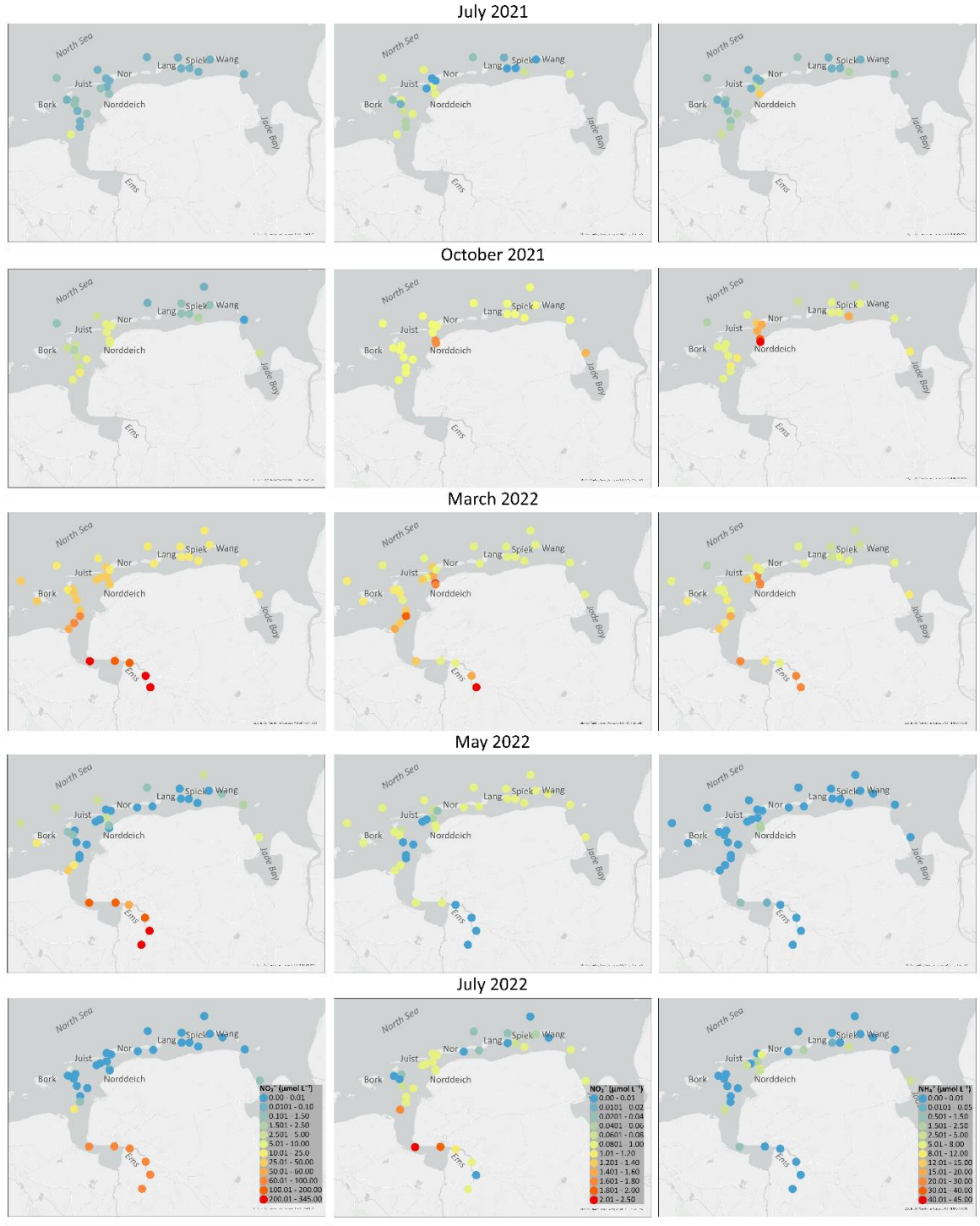

445

Figure 12: Measured nitrate (NO_3^- in µmol L^{-1}), nitrite (NO_2^- in µmol L^{-1}) and ammonium (NH_4^+ in µmol L^{-1}) of all seasonal cruises from July 2021 until July 2022. The map in this Figure was generated using ArcGIS. Data sources: LGLN, Esri, TomTom, Garmin, Foursquare, FAO, METI/NASA, USGS. © 2024 Julia Meyer.

https://doi.org/10.5194/egusphere-2024-3048
Preprint. Discussion started: 23 October 2024

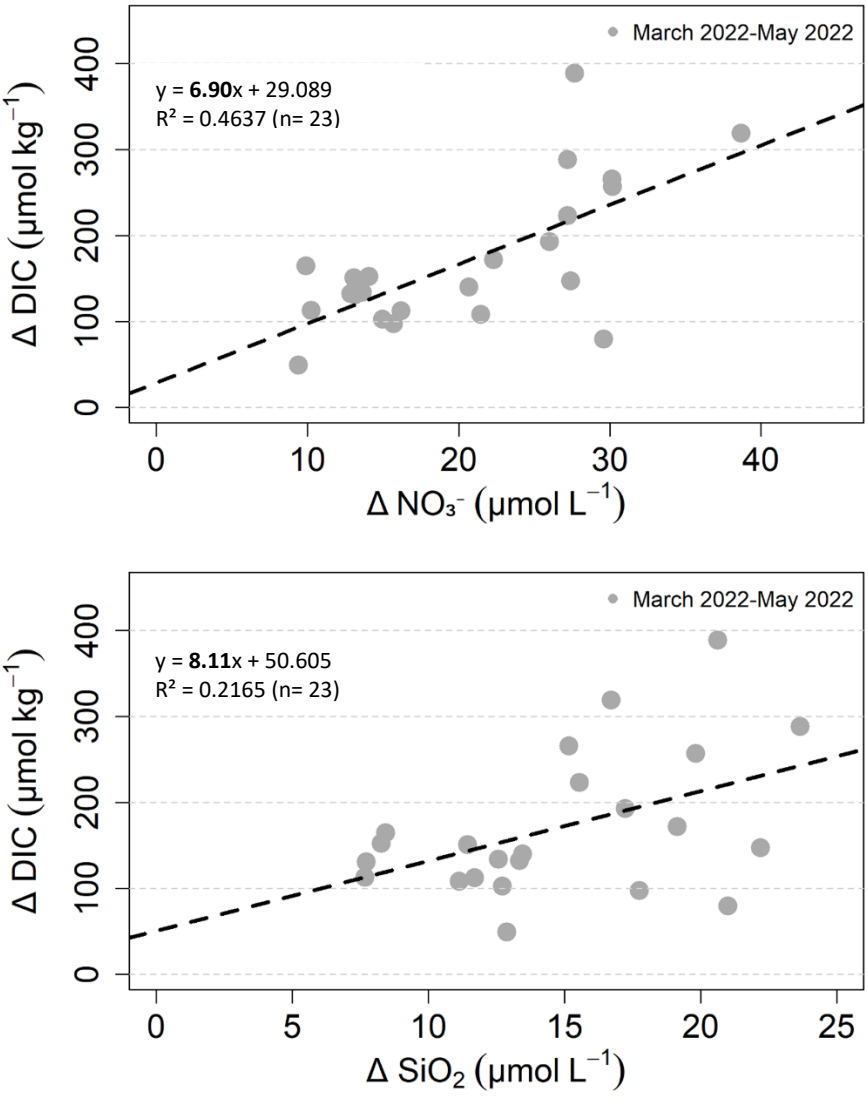

Figure 13: NO_3^- and SiO_2 differences (ΔNO_3^-, ΔSiO_2) of March to May 2022 against the difference of DIC (ΔDIC), with the related regression equations. The slopes show the Redfield Ratios of all measured stations in the Western and Eastern WS.

4 Discussion

4.1 Regional and seasonal Differences in the Carbonate System of the East Frisian Wadden Sea

Coastal oceans and shelf seas, such as the North Sea, exhibit significant variability (Blackford and Gilbert, 2007), a phenomenon also observed in the carbonate system of the East Frisian WS. The study highlights regional and seasonal

https://doi.org/10.5194/egusphere-2024-3048
Preprint. Discussion started: 23 October 2024

variability in the carbonate system of the East Frisian WS. Notably, there is a pronounced West-to-East gradient in DIC and TA, with both showing considerable fluctuations across seasons.

Seasonal biological production appears to enhance TA, especially in spring and summer, potentially increasing the region's capacity for carbon dioxide uptake. However, the TA variability in the coastal ocean is more complex, due to other processes like evaporation, coastal shelf circulation and tidal dynamics, upwelling, sulfate reduction, denitrification, nitrification and calcium carbonate calcification and dissolution (Abril et al., 2003; Böttcher et al., 1998; Brewer and Goldman, 1976; Cai et al., 2010; Cao et al., 2011; Chen and Wang, 1999; Faber et al., 2014; Hoppema, 1990; Liu et al., 2012; Onken and Riethmüller, 2010; Postma, 1981; Voynova et al., 2019; Wolf-Gladrow et al., 2007).

4.2 [TA-DIC] as a proxy for Biogeochemical Processes Driving Carbonate Dynamics

Previous studies have shown that [TA-DIC] can be used to identify the influence in biogeochemical processes, for instance $CaCO_3$ precipitation/ formation, photosynthesis, respiration and therefore CO_2 uptake and release (Xue and Cai, 2020) (Fig. 14; Fig. 15), and that it can be used as a good proxy for these processes even in coastal oceans (Xue and Cai, 2020). The advantage is that this parameter is independent of ocean mixing and is not sensitive to temperature and pressure changes (Xue and Cai, 2020), which makes it a good tracer for larger-scale oceanographic studies, as well as suitable for seasonal observations of biogeochemical processes and carbonate dynamics of an ecosystem. The difference, [TA-DIC], can better reflect variations on $[CO_3^{2-}]$ compared to the ratio of TA and DIC [TA:DIC] (Xue et al., 2017).

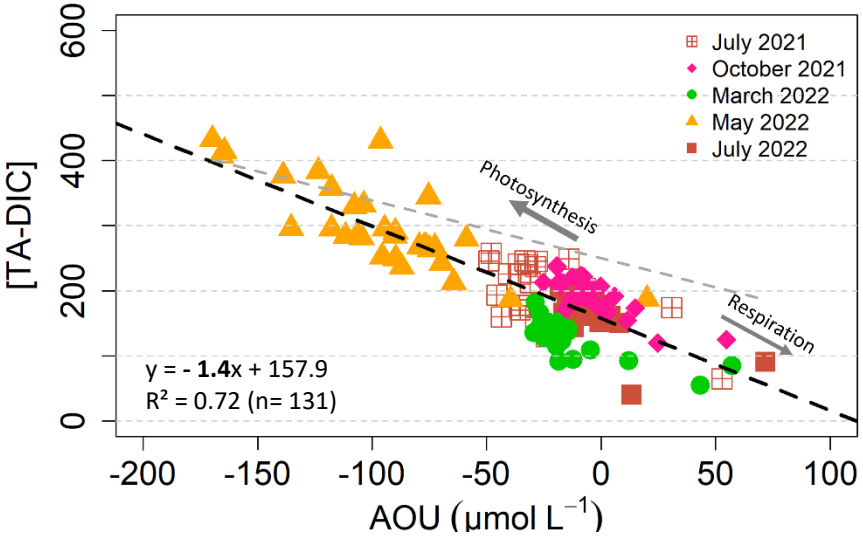

Figure 14: AOU relationship to [TA-DIC] in µmol kg^{-1} of all seasonal cruises with the related regression analysis (black dashed line). The arrows show the possible processes that could affect the [TA-DIC] and apparent oxygen utilization (AOU). The grey dashed line represents the regression line, which illustrates the Redfield ratio slope (- 123/138 = -0.89), proposed by (Xue and Cai, 2020).

Figure 14 presents data from all stations in the WS sampled during different seasons and the calculated AOU relationship to [TA-DIC], which we can directly link to the Redfield ratio (Redfield, 1963). This information is essential to understand the

https://doi.org/10.5194/egusphere-2024-3048
Preprint. Discussion started: 23 October 2024

role of the biological carbon pump and the influence on biogeochemical processes (Xue and Cai, 2020). However, it is important to note that these samples were collected exclusively during daylight hours, excluding the night cycle. This likely skews the data towards conditions that favor photosynthesis over respiration, as photosynthesis occurs during the daylight hours, while respiration continues both day and night. We therefore measured predominantly negative AOU values and an increase in [TA-DIC] due to reduced DIC (Fig. 14). The microphytobenthos in the Northern German WS for example was found to significantly impact the local carbon cycle through photosynthesis, producing oxygen and consuming CO_2 during the day (Wolfstein et al., 2000). This aligns with the observed negative AOU values and higher [TA-DIC], as photosynthesis would rise [TA-DIC] by consuming CO_2 and generating oxygen, thus affecting AOU (Fig. 14). In contrast, respiration, which occurs continuously both day and night, increases AOU, leading to positive values, and decreases [TA-DIC], as more dissolved inorganic carbon is produced through the decomposition of organic material. Specifically, the respiration of 1 mole of organic matter ($(CH_2O)_{106}(NH_3)_{16}H_3PO_4$) increases DIC by 106 moles and decreases TA by 17 moles (Chen 1978). This results in a change of 123 moles in [TA-DIC] (Xue and Cai, 2020).

The regression of Fig. 14 shows a negative correlation between [TA-DIC] and AOU with a negative slope of - 1.416 µmol kg^{-1} per µmol L^{-1} AOU. This slope is steeper than the Redfield ratio slope (- 123/138 = - 0.89), as proposed by (Xue and Cai 2020), which is based on conditions dominated by aerobic respiration and production. The steeper slope observed in the East Frisian WS suggests deviations from these typical conditions, indicating that the biogeochemical processes in this region may differ from those assumed in the Redfield model (Fig. 14). Variations in production and respiration, including Photosynthetic Quotient (PQ) and Respiratory Quotient (RQ) (Gazeau et al., 2005; Hopkinson and Smith, 2005), as well as the variability of the physiological status of different algae species (Wolfstein et al., 2000) could contribute to this deviation and can influence the observed slope. This may also be caused by specific local environmental conditions or deviating biogeochemical processes. Therefore, Xue and Cai (2020) assumed that this is due to higher tendency of dissolution of $CaCO_3$, which has been suggested as a source for increasing TA (Norbisrath et al., 2023), where the authors assumed that TA was produced in the sediments through anaerobic processes and $CaCO_3$ dissolution, and concluded that the Dutch Wadden Sea can be a potential source for TA (Norbisrath et al., 2023). This can contribute to TA generation in the East Frisian WS as well, especially in summer in the Western part. It has been hypothesized that TA generation within the Wadden Sea may have an important effect on the carbon storage capacity of the North Sea (Burt et al., 2016; Schwichtenberg et al., 2020) and thus on carbon dynamics, therefore the seasonal dynamics we observe can modulate this effect.

Figure 15 indicates a mix of the dominate processes of respiration and CO_2 uptake during this season. This can also be seen in the increasing $pCO_{2\ obs}$ concentrations (Fig. 4). However, when we analyze the nutrient content during this season, higher NO_3^- concentrations were measured (Fig. 12; Fig. 13). Nitrification involves the conversion of NH_4^+ to NO_2^-, causing a decrease of TA by 2 moles per mole N, through the oxidation of ammonia to NO_2^-. In addition, the nitrogen fixation could decrease TA by 1 mole per mole of N. The process consumes hydrogen ions (H^+) and releases hydroxide ions (OH^-), leading to an increase of pH (Brenner et al. 2016). This could indicate a possible mix of these processes in addition to respiration and $CaCO_3$ dissolution in March 2022, controlling the carbonate dynamics in the intertidal region of the East Frisian WS (Fig.15). In

https://doi.org/10.5194/egusphere-2024-3048
Preprint. Discussion started: 23 October 2024

October 2021, [TA-DIC] < 200 µmol kg^{-1} are found, suggesting respiration and CO_2 release during this season (Fig. 14; Fig. 15). The uptake of CO_2 from the atmosphere by the ocean can increase DIC, but not TA, followed by a decreasing [TA-DIC] (Xue and Cai 2020).

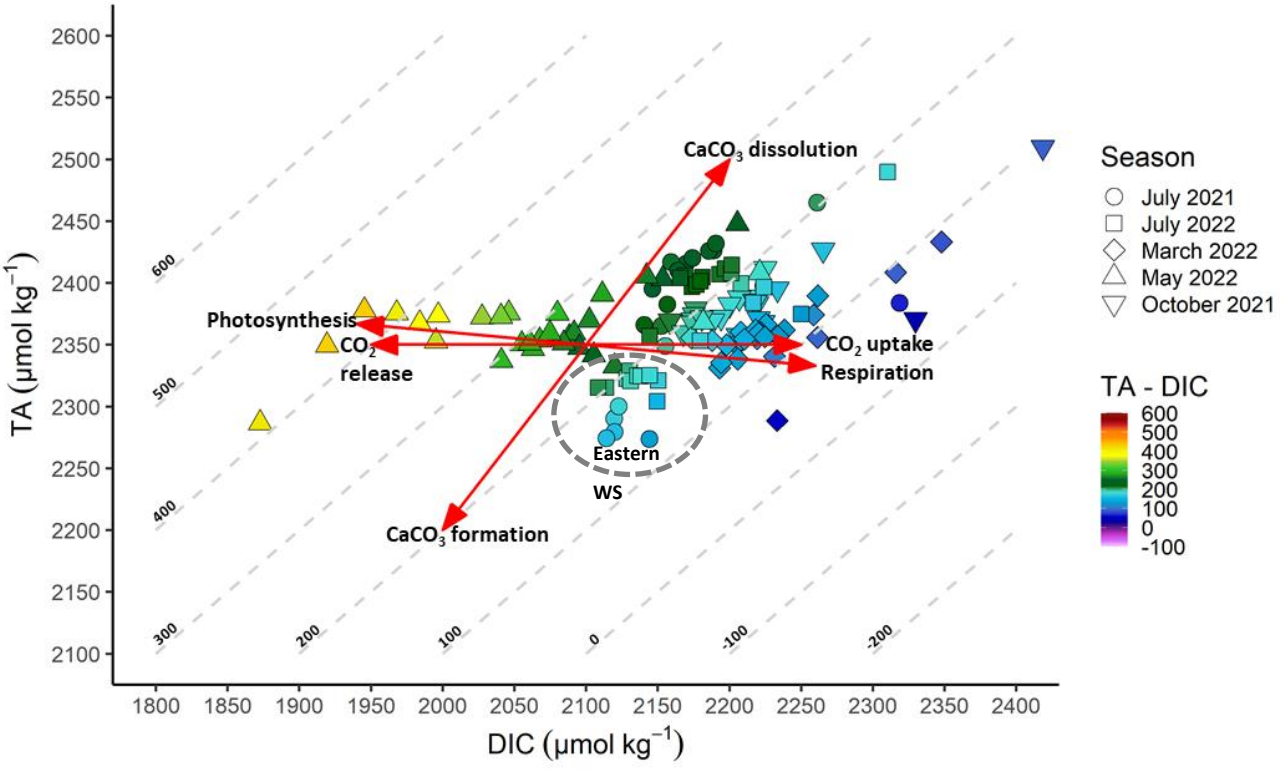

Figure 15: DIC versus TA plot from all seasons, with the colored value of [TA-DIC] in µmol kg^{-1} from the intertidal region with salinity 25-32.5. The isoclines are representing the [TA-DIC] values. The red lines showing the related biogeochemical processes (Photosynthesis, Respiration, CO_2 release and CO_2 uptake and $CaCO_3$ formation / dissolution), that could cause the changes in TA and DIC in the intertidal region of the intertidal East Frisian Wadden Sea. The Eastern part of the East Frisian is highlighted here with the dotted grey cycle.

Higher TA concentrations were found in summer, where compared to the North Sea, the TA concentrations in the WS were higher (> 2489 µmol kg^{-1}), suggesting a generation of TA in the intertidal WS (Fig. 7; Fig. 8). In the summer (July 2021, July 2022), [TA-DIC] values (< 200 µmol kg^{-1}) from the Eastern WS are located under the respiration/photosynthesis line (Fig. 14; Fig. 15). In contrast, the measured [TA-DIC] concentrations in the Western WS in summer are > 200 µmol kg^{-1} (Fig. 15), and above the respiration/photosynthesis fit.

In July 2022, the salinity in the same region changed by 2 - 3 units from one day (July 11) to another (July 12), where the salinity was higher in the East (Fig. 2), leading to the slightly higher measured TA values (+53.7 ± 36.7 µmol kg^{-1}) in July 2022, compared to the previous year (Table 3). On the sampling day July 11, the sluice in Neuharlingersiel was opened just before we started our sampling. Due to this anthropogenic influence, it is reasonable to treat these July 11 measurements as

https://doi.org/10.5194/egusphere-2024-3048
Preprint. Discussion started: 23 October 2024

anomalies, potentially influenced by the sudden changes in salinity and local hydrological conditions. However, higher temperatures in summer also enhances evaporation, which could have an impact on TA and salinity, both would increase as a result (Schneider et al., 2007). A study by Onken and Riethmüller (2010), showed that evaporation in the tidal flats of the WS raised salinity by 0.65 within just 3.5 hours, indicating that tidal flats experience intensified evaporation during warmer months compared to other areas. This can also be seen in the stations with higher salinities (~ 32) of the Eastern intertidal WS, which can be identified with lower [TA-DIC] (< 200 µmol kg^{-1}) values and the Western stations with lower salinity and thus slightly higher [TA-DIC] values (Fig. 14; Fig. 15). Consequently, it is likely that $CaCO_3$ formation occurs in the Eastern WS, as indicated by its Ωcal of 1.9 ± 0.8, while $CaCO_3$ dissolution is more prevalent in the Western part of the East Frisian WS, which has a Ωcal of 3.8 ± 0.4 (Fig. 15). This suggests a favorable environment for calcite formation in the Western WS, whereas the Eastern WS, while still supersaturated, may experience conditions that lean toward dissolution. $CaCO_3$ formation by 1 mole is known to decrease TA by 2 moles, changing [TA-DIC] by 1 mole (Xue and Cai 2020). In contrast, as $CaCO_3$ dissolves, TA and DIC increases and [TA-DIC] increases by 1 mole. The same regional variability is observed in July 2021 (Fig. 7. Fig.8), suggesting that $CaCO_3$ dissolution dominates and generates TA in the Western WS (Fig. 15). This TA generation in summer can change the buffer capacity, allowing for the Western WS to potentially take up or store carbon (Fig.15) (Gruber et al., 2019; Li et al., 2024), compared to other seasons, and despite the southern North Sea being considered in general as a carbon source to the atmosphere (Thomas et al. 2009; Voynova et al. 2019). This also suggests that the intertidal regions of the Western Frisian WS can be a source of TA to the coast in the summer, as previously proposed by (Thomas et al. 2009; Voynova et al. 2019).

In contrast, in spring (May 2022) the high rates of photosynthesis, suggested by low $pCO_{2\,obs}$, high dissolved oxygen, pH and chlorophyll values (Fig. 3;Fig. 4) (Artioli et al., 2012; Thomas et al., 2005b), result in a decrease in AOU (down to - 169 µmol L^{-1}) over the day (Table 2; Fig. 14) and an increased [TA-DIC], due to the substantial drawdown of DIC in May 2022 (Fig. 7; Fig. 14; Fig. 15). This indicates that this region is a sink for CO_2 due to carbon fixation and nitrate assimilation (Borges et al., 2005). A decline of AOU can significantly change the DIC concentration and consequently increase [TA-DIC] values, which was the case during the productive seasons (July 2021, July 2022, May 2022).

Strong biological production reduced DIC concentrations, indicating consumption of inorganic carbon with DIC falling below to the mixing line (Fig. 8), and $pCO_{2\,obs}$ reaching levels of < 200 µatm (Fig. 4). This can also be seen in Fig. 14, where the May measurements follow roughly the photosynthesis/respiration line, indicated by the progressively low DIC values in May (Fig. 7). At the same time, TA also increased slightly during this period, as indicated by the slight deviation from the photosynthesis/respiration line (Fig. 14), increasing from March 2022 to May 2022 by approximately 9.1 ± 29.2 µmol kg^{-1} in the intertidal regions, above the mixing line (Fig. 8). This suggests a slight production of TA compared to March 2022. The relationship in Fig. 12 also indicates that primary production is influenced by nitrate and silicate availability. Overall, the data confirm that primary production leads to a significant decrease in DIC, which is reflected in the changes in nutrient concentrations, as well as a slight production of TA (Fig. 7; Fig. 8; Fig. 13).

https://doi.org/10.5194/egusphere-2024-3048
Preprint. Discussion started: 23 October 2024

We therefore propose that assimilation of NO_3^- during the time of intense primary production in May 2022 could explain the local increase of total alkalinity during the spring bloom. First, the maximum concentration of NO_3^- was captured in March before the high biologically productive season started in May 2022 (Fig. 11 -15), with maximum concentrations measured in the Western WS. A significant drawdown of NO_3^- in the intertidal regions from the maximum value of 65 µmol kg^{-1} in March 2022 to 22 µmol kg^{-1} in May 2022, resulted in an average decrease of 19.2 ± 9.6 µmol kg^{-1} of NO_3^- (Fig. 12; Fig. 13). An uptake of NH_4^+ was not obvious, because NH_4^+ concentrations were much lower during this period (Fig. 12), suggesting only a small impact on TA patterns. In contrast, the decrease of NO_3^- from May 2022 to July 2022 was smaller in comparison (1.51 ± 5.16 µmol kg^{-1}, Fig. 12). However, generally the NO_3^- concentration is low in summer, which was due to higher turnover rates (Kieskamp et al. 1991). Since denitrification is dependent on nitrate supply, previous studies identified lower denitrification rates seasonally in summer (Kieskamp et al. 1991; Faber et al. 2014). Due to the high oxygen concentrations in the intertidal East Frisian WS, anaerobic denitrification, which can increase TA (Chen and Wang, 1999), is unlikely in the water column, but can take place in the sediments (not addressed in this study).

4.3 Biological and thermal pCO_2 dynamics

Previous work demonstrated that the most significant temporal variability in the ocean surface pCO_2 is seasonal, linked to either thermal or non-thermal factors (Takahashi et al., 1993, 2002). The pCO_2 changes approximately 4.2 % for every 1°C change in temperature, increasing with warmer sea surface temperature (SST) and decreases with colder SST (Takahashi et al., 1993).

Seasonal changes in the observed, biological and thermal components of pCO_2 were observed in the East Frisian WS in the Eastern and Western WS (Fig. 6). The temperature on March 2022 was low (3.89 - 6.47 °C) (Fig. 2), reducing the solubility of pCO_2 (Prowe et al. 2009). This was also the season in which the lowest $pCO_{2\ therm}$ (453 µatm) was measured (Fig. 6). The biological component of $pCO_{2\ bio}$ was relatively high in comparison (see section 3.1.2). However, the NO_3^- concentration measured in March 2022 was also higher (Fig. 12) in comparison.

Especially in May 2022, low $pCO_{2\ obs}$ values (down to 141.3 µatm) close to the calculated $pCO_{2\ bio}$ values were measured (Fig. 6), suggesting a biological control of primary producers. The average measurement of $pCO_{2\ obs}$ agrees seasonally well with other studies in the North Sea (Prowe et al. 2009; Macovei et al. 2021), where $pCO_{2\ obs}$ dropped constantly during spring season and increased during early summer (Fig. 6). The $pCO_{2\ obs}$ and DIC decreased, as a result of the production of organic matter by primary producers (Macovei et al. 2021) in May 2022 (Fig. 4 Fig. 6). In contrast, in July 2022, an increase in pCO_2 was observed, attributed to the remineralization of organic material (Macovei et al. 2021; Artioli et al. 2012) , but also an increase in surface water temperatures in July (Fig. 6). During remineralization, organic matter is broken down, releasing CO_2. Simultaneously, the data show that Ωcal was relatively high (Table 2; Fig. 5). Additionally, lower DIC concentrations were measured, which could indicate enhanced primary production or another CO_2-consuming process. Similar results were also found in previous studies, which defines thermal effects, reduced mixing, remineralization and CO_2 uptake by phytoplankton as possible drivers of seasonal high pCO_2 observed in the North Sea in summer (Prowe et al. 2009).

https://doi.org/10.5194/egusphere-2024-3048
Preprint. Discussion started: 23 October 2024

Lower salinity water masses (> 25) contained higher $pCO_{2\ obs}$ concentrations during all seasons, which suggests a possible riverine input of higher pCO_2 water mass coming from the Ems and Weser River estuaries (Fig. 2), especially in the wet seasons. Regionally, the measured $pCO_{2\ obs}$ was low in the intertidal East Frisian WS compared to the high turbid Ems River estuary in summer (July 2021, July 2022, May 2022). Previous studies also found this pattern of lower salinity water masses related to pCO_2 concentrations with increase pCO_2 concentrations where water masses of runoff enter the North Sea (Burt et al. 2016; Thomas et al. 2005a).

4.4 Additional Factors affecting TA and DIC Dynamics

Particularly, the tidal WS plays an important role in the biogeochemical cycling of the North Sea (Santos et al., 2015; Thomas et al., 2009), because many European rivers empty in the WS (Thomas et al. 2009). A few studies discussed the generation in of TA in summer before (Schwichtenberg, 2013; Voynova et al., 2019), however in summer the riverine inflow is lowest, which could not explain an increase of TA in the WS.

This observation is supported by the ΔTA_{excess} values, where the riverine mixing effect was removed (Fig. 10), showing a similar pattern as the mixing plots in summer in the Western WS (Fig. 8). Nonetheless, the TA values measured in March 2022 and the ΔTA_{excess} (Fig. 8; Fig. 10) values indicating a mixing effect of riverine water masses coming from the Ems River estuary (Fig. 10), due to the inconsistency in comparison to the mixing plots (Fig. 8c). The highest riverine contribution of TA is expected from January to April (Pätsch and Lenhart, 2004; Schwichtenberg, 2013). However, the moderate rainfall and cooler-than-average weather in October 2021 may have influenced the hydrology of the region, potentially causing increased terrestrial runoff and enhanced delivery of alkalinity-rich water to the coastal system. This would contrast with drier, warmer periods, where evaporation and lower river discharge would dominate (Onken and Riethmüller, 2010).

The tidal dynamics of the WS can also play a crucial role in regulating biogeochemical processes. The tidal flats may experience intensified cycling of carbonates, particularly in transitional seasons like autumn when temperature and biological activity are still relatively high. This could contribute to an accumulation of TA in the system (Thomas et al., 2009). Internal processes within the WS, such as carbonate dissolution or sediment reworking, could also explain the higher TA values (Brenner et al., 2016; Burt et al., 2014; Van Dam et al., 2022; Norbisrath et al., 2023; Thomas et al., 2009). These processes may be more pronounced in autumn as biological and chemical activity shifts with the changing seasons. Previous studies, like Schwichtenberg (2013), suggest that riverine loads account for only about 9% of TA variability in the German Bight. However, localized weather events and specific regional conditions in autumn might enhance the riverine contribution during certain periods.

Previous studies (Hoppema, 1990; Norbisrath et al., 2023) have observed an increase in TA and DIC from high to low tide over a tidal cycle in the Wadden Sea. However, this study could not sample all stations during low tide, so it is not possible to capture the complete tidal patterns here. This means that some of the results might be affected by tidal changes, with an average increase of 51.6 µmol kg^{-1} in TA and 101.3 µmol kg^{-1} in DIC during ebb tide, as proposed before (Norbisrath et al., 2023). In contrast, the Ωcal was highest at high tide (3.8) and lowest at ebb tide (3.1) in the Dutch Wadden Sea (Norbisrath et al., 2023). The intertidal East Frisian WS in this study was mostly sampled during low or rising tide, whereas the stations more offshore

https://doi.org/10.5194/egusphere-2024-3048
Preprint. Discussion started: 23 October 2024

(behind the Islands) and the stations in the Jade Bay (Fig. 1) mostly were sampled during high tide. The stations in the Western part of the East Frisian WS were mainly sampled during rising tide during all seasonal cruises. However, a slight variation in sampling times could not be avoided, which may explain some of the observed TA dynamics in the Western WS, particularly the increased influence of sediments at low tides (Norbisrath et al., 2023). Therefore, $CaCO_3$ dissolution at the water-sediment interface, where TA is remineralized (Norbisrath et al., 2023) could be an important driver for these dynamics. The transect from Norddeich harbour to Norderney, sampled during ebb or declining tide across all seasons, also exhibited notable patterns in TA and DIC, potentially influenced by tidal changes. Therefore, the higher TA and DIC values observed (Table 3; Fig. 7), particularly in October 2021, may be linked to sediment interaction and carbonate dissolution, highlighting the crucial role of tidal and sedimentary dynamics (Norbisrath et al., 2023) in shaping these biogeochemical parameters.

5 Conclusions

This study highlights the regional and seasonal variations in the carbonate system of the East Frisian Wadden Sea, reflecting on the carbon dynamics of coastal and shelf seas. The findings reveal that both total alkalinity (TA) and dissolved inorganic carbon (DIC) vary substantially across different regions and seasons, with a notable decrease in DIC from East to West and an increase in TA during biologically productive periods such as spring and summer.

In spring 2022, a significant drawdown of NO_3^- was observed, correlating with a slight increase in TA, likely due to nitrate assimilation during primary production. The generation of TA in the Western East Frisian Wadden Sea, particularly in summer, suggests that this region may play a role in carbon storage. The higher TA concentrations observed in summer, coupled with the processes of $CaCO_3$ dissolution, indicate that the Western WS could act as a source of TA to the adjacent coastal waters. This TA generation may enhance the region's capacity to absorb CO_2, despite the broader southern North Sea generally being considered a carbon source to the atmosphere. Analyzing changes in ΔTA_{excess}, ΔDIC_{excess} and ΔTA_P helps better understand seasonal patterns and the underlying biogeochemical processes and mixing. The riverine input - which could have been a possible driver for TA production in the tidal driven East Frisian Wadden Sea – was excluded as a dominate reason, due to the low riverine input during the warm seasons. Nevertheless, higher inputs of riverine water masses can strongly influence TA and DIC in coastal regions and should not be ignored in such studies, like in March 2022 in this study. Primary production in May 2022 could explain up to 80 % of the ΔDIC_{excess} in the Western WS and up to 90 % ΔDIC_{excess} in the Eastern WS, which resulted in such an extreme drop in DIC, slight production in TA and drawdown in NO_3^- during this period.

The results of the present study successfully applied the parameter [TA-DIC] to explain seasonal and regional changes in TA and DIC in the East Frisian Wadden Sea caused by biogeochemical processes in a coastal system. Understanding the described biogeochemical dynamics is crucial for predicting the impact of climate change on coastal and shelf seas, where variability in TA and DIC can influence the regional carbon cycling and contribute to broader oceanic carbon dynamics. However, in a tidal system such as the East Frisian Wadden Sea, additional factors such as nutrient loading, groundwater discharge, riverine input, tides as well as sediment-pelagic coupling should also considered.

https://doi.org/10.5194/egusphere-2024-3048
Preprint. Discussion started: 23 October 2024

The observed regional and seasonal variability in the carbonate system of the East Frisian Wadden Sea reveals complex biogeochemical processes that are influenced by tidal cycles, riverine inputs, and sediment interactions. These dynamics highlight the regional and seasonal factors when assessing the carbonate capacity and carbon dynamics of coastal ecosystems like the Wadden Sea. Tidal variations, though not fully captured in the study, significantly impact TA and DIC concentrations, with ebb tides typically showing higher levels due to sediment interactions and $CaCO_3$ dissolution. Riverine inputs, particularly from the Ems River estuary, also shape the local carbonate chemistry, though low summer inflows suggest that sediment interactions may play a larger role. To fully understand these intricate interactions and their implications for carbon storage and marine biogeochemistry in this ecologically significant region, further research, including sediment studies and continuous tidal monitoring, is essential.

Code and data availability

The data supporting our findings within this study have been submitted by Lara Luitjens (NLWKN) to PANGAEA data repository and are currently undergoing final editorial processing. A DOI for the dataset will be available upon completion of the review process.

Competing interests

The contact author has declared that none of the authors has any competing interests.

Acknowledgements

We deeply appreciate the laboratory technicians Martina Gehrung, Tanja Pieplow and Catharina Petrauskas for their exceptional technical support, meticulous work and dedication. They ensured the reliability and accuracy of our data through their careful handling of samples and precise analytical measurements. The scientists and crew who participated in the research expeditions, including the captain Alexander Heidenreich and the crew of the *RV Burchana* (Jens Voß and Winfried Bruns) are also greatly appreciated. It was their hard work, professionalism and co-operation during the challenging field work that made it possible to collect the data required for this study. The success of our research would not have been possible without your tireless efforts at sea. We thank all of you for your unwavering support and commitment.

Finally, we would like to acknowledge the support and valuable discussions with the members of the ”CARBOSTORE” project and especially Dr. habil. Michael Böttcher from the Institute for Baltic Sea Research in Warnemünde (Germany).

Financial support

This research was funded through the “CARBOSTORE” project (Grant Number 03F0875A), by the German Federal Ministry of Education and Research (BMBF). Additionally, the Helmholtz-Zentrum Hereon covered the article processing charges for this open-access publication.

https://doi.org/10.5194/egusphere-2024-3048
Preprint. Discussion started: 23 October 2024

References

4H - Jena engineering GmbH: Data Processing for CONTROS HydroC© CO_2 (Manual), 2021.

Abril, G., Etcheber, H., Delille, B., Frankignoulle, M., and Borges, A. V.: Carbonate dissolution in the turbid and eutrophic Loire estuary, Mar Ecol Prog Ser, 259, 129–138, https://doi.org/10.3354/meps259129, 2003.

Al-Raei, A. M., Bosselmann, K., Böttcher, M. E., Hespenheide, B., and Tauber, F.: Seasonal dynamics of microbial sulfate reduction in temperate intertidal surface sediments: controls by temperature and organic matter, Ocean Dyn, 59, 351–370, https://doi.org/10.1007/s10236-009-0186-5, 2009.

Artioli, Y., Blackford, J. C., Butenschön, M., Holt, J. T., Wakelin, S. L., Thomas, H., Borges, A. V., and Allen, J. I.: The carbonate system in the North Sea: Sensitivity and model validation, Journal of Marine Systems, 102–104, 1–13, https://doi.org/10.1016/j.jmarsys.2012.04.006, 2012.

Bauer, J. E., Cai, W. J., Raymond, P. A., Bianchi, T. S., Hopkinson, C. S., and Regnier, P. A. G.: The changing carbon cycle of the coastal ocean, Nature, 504, https://doi.org/10.1038/nature12857, 2013.

Van Beusekom, J. E. E. and De Jonge, V. N.: Long-term changes in Wadden Sea nutrient cycles: Importance of organic matter import from the North Sea, Hydrobiologia, 475–476, 185–194, https://doi.org/10.1023/A:1020361124656, 2002.

Blackford, J. C. and Gilbert, F. J.: pH variability and CO_2 induced acidification in the North Sea, Journal of Marine Systems, 64, 229–241, https://doi.org/10.1016/j.jmarsys.2006.03.016, 2007.

Borges, A. V., Delille, B., and Frankignoulle, M.: Budgeting sinks and sources of CO_2 in the coastal ocean: Diversity of ecosystem counts, Geophys Res Lett 32, 1–4, https://doi.org/10.1029/2005GL023053, 2005.

Böttcher, M. E., Oelschläger, B., Höpner, T., Brumsack, H. J., and Rullkötter, J.: Sulfate reduction related to the early diagenetic degradation of organic matter and "black spot" formation in tidal sandflats of the German Wadden Sea (southern North Sea): Stable isotope (^{13}C, ^{34}S, ^{18}O) and other geochemical results, Org Geochem, 29, 1517–1530, https://doi.org/10.1016/S0146-6380(98)00124-7, 1998.

Brenner, H., Braeckman, U., Le Guitton, M., and Meysman, F. J. R.: The impact of sedimentary alkalinity release on the water column CO_2 system in the North Sea, Biogeosciences, 13, 841–863, https://doi.org/10.5194/bg-13-841-2016, 2016.

Brewer, P. G. and Goldman, J. C.: Alkalinity changes generated by phytoplankton growth, Limnol Oceanogr, 21, 108–117, https://doi.org/10.4319/lo.1976.21.1.0108, 1976.

Burt, W. J., Thomas, H., Pätsch, J., Omar, A. M., Schrum, C., Daewel, U., Brenner, H., and De Baar, H. J. W.: Radium isotopes as a tracer of sediment-water column exchange in the North Sea, Global Biogeochem Cycles, 28, 786–804, https://doi.org/10.1002/2014GB004825, 2014.

Burt, W. J., Thomas, H., Hagens, M., Pätsch, J., Clargo, N. M., Salt, L. A., Winde, V., and Böttcher, M. E.: Carbon sources in the North Sea evaluated by means of radium and stable carbon isotope tracers, Limnol Oceanogr, 61, 666–683, https://doi.org/10.1002/lno.10243, 2016.

https://doi.org/10.5194/egusphere-2024-3048
Preprint. Discussion started: 23 October 2024

Cai, W. J., Hu, X., Huang, W. J., Jiang, L. Q., Wang, Y., Peng, T. H., and Zhang, X.: Alkalinity distribution in the western North Atlantic Ocean margins, J Geophys Res Oceans, 115, https://doi.org/10.1029/2009JC005482, 2010.

Cao, Z., Dai, M., Zheng, N., Wang, D., Li, Q., Zhai, W., Meng, F., and Gan, J.: Dynamics of the carbonate system in a large continental shelf system under the influence of both a river plume and coastal upwelling, J Geophys Res Biogeosci, 116, https://doi.org/10.1029/2010JG001596, 2011.

Chen, C. T. A. and Wang, S. L.: Carbon, alkalinity and nutrient budgets on the East China Sea continental shelf, J Geophys Res Oceans, 104, 20675–20686, https://doi.org/10.1029/1999jc900055, 1999.

Chen, C.-T. A.: Decomposition of Calcium Carbonate and Organic Carbon in the Deep Oceans, Science, 201, 735–736, https://doi.org/10.1126/science.201.4357.735, 1978.

Chierici, M., Fransson, A., and Nojiri, Y.: Biogeochemical processes as drivers of surface fCO_2 in contrasting provinces in the subarctic North Pacific Ocean, Global Biogeochem Cycles, 20, https://doi.org/10.1029/2004GB002356, 2006.

Van Dam, B. R., Crosswell, J. R., Anderson, I. C., and Paerl, H. W.: Watershed-Scale Drivers of Air-Water CO_2 Exchanges in Two Lagoonal North Carolina (USA) Estuaries, Journal of Geophysical Research: Biogeosciences, 123, 271–287, https://doi.org/10.1002/2017JG004243, 2018.

Van Dam, B., Lehmann, N., Zeller, M. A., Neumann, A., Pröfrock, D., Lipka, M., Thomas, H., and Böttcher, M. E.: Benthic alkalinity fluxes from coastal sediments of the Baltic and North seas: comparing approaches and identifying knowledge gaps, Biogeosciences, 19, 3775–3789, https://doi.org/10.5194/bg-19-3775-2022, 2022.

Dickson, A. G.: An exact definition of total alkalinity and a procedure for the estimation of alkalinity and total inorganic carbon from titration data, Deep Sea Research Part A. Oceanographic Research Papers, 28, 609–623, https://doi.org/10.1016/0198-0149(81)90121-7, 1981.

Dickson, A. G., Afghan, J. D., and Anderson, G. C.: Reference materials for oceanic CO_2 analysis: a method for the certification of total alkalinity, Mar Chem, 80, 185–197, https://doi.org/10.1016/S0304-4203(02)00133-0, 2003.

Dickson, A. G., Sabine, C. L., Christian, J. R., and North Pacific Marine Science Organization.: Guide to best practices for ocean CO_2 measurements, North Pacific Marine Science Organization, 2007.

Faber, P. A., Evrard, V., Woodland, R. J., Cartwright, I. C., and Cook, P. L. M.: Pore-water exchange driven by tidal pumping causes alkalinity export in two intertidal inlets, Limnol Oceanogr, 59, 1749–1763, https://doi.org/10.4319/lo.2014.59.5.1749, 2014.

Feely, R., Doney, S., and Cooley, S.: Ocean Acidification: Present Conditions and Future Changes in a High-CO_2 World, Oceanography, 22, 36–47, https://doi.org/10.5670/oceanog.2009.95, 2009.

Friedlingstein, P., O'Sullivan, M., Jones, M. W., Andrew, R. M., Bakker, D. C. E., Hauck, J., et al.: Global Carbon Budget 2023, Earth Syst Sci Data, 15, 5301–5369, https://doi.org/10.5194/essd-15-5301-2023, 2023.

Gattuso, J. P., Frankignoulle, M., and Wollast, R.: Carbon and carbonate metabolism in coastal aquatic ecosystems, Annu Rev Ecol Syst, 29, 405–434, https://doi.org/10.1146/annurev.ecolsys.29.1.405, 1998.

https://doi.org/10.5194/egusphere-2024-3048
Preprint. Discussion started: 23 October 2024

Gazeau, F., Borges, A., Barrón, C., Duarte, C., Iversen, N., Middelburg, J., Delille, B., Pizay, M., Frankignoulle, M., and Gattuso, J.: Net ecosystem metabolism in a micro-tidal estuary (Randers Fjord, Denmark): evaluation of methods, Mar Ecol Prog Ser, 301, 23–41, https://doi.org/10.3354/meps301023, 2005.

Grasshoff, K., Kremling, K., and Ehrhardt, M.: Methods of Seawater Analysis, edited by: Grasshoff, K., Kremling, K., and Ehrhardt, M., Wiley, https://doi.org/10.1002/9783527613984, 1999.

Gruber, N., Clement, D., Carter, B. R., Feely, R. A., van Heuven, S., Hoppema, M., Ishii, M., Key, R. M., Kozyr, A., Lauvset, S. K., Lo Monaco, C., Mathis, J. T., Murata, A., Olsen, A., Perez, F. F., Sabine, C. L., Tanhua, T., and Wanninkhof, R.: The oceanic sink for anthropogenic CO_2 from 1994 to 2007, Science, 363, 1193–1199, https://doi.org/10.1126/science.aau5153, 2019.

Grunwald, M., Dellwig, O., Beck, M., Dippner, J. W., Freund, J. A., Kohlmeier, C., Schnetger, B., and Brumsack, H. J.: Methane in the southern North Sea: Sources, spatial distribution and budgets, Estuar Coast Shelf Sci, 81, 445–456, https://doi.org/10.1016/j.ecss.2008.11.021, 2009.

Hopkinson, C. S. and Smith, E. M.: Estuarine respiration: an overview of benthic, pelagic, and whole system respiration, in: Respiration in Aquatic Ecosystems, Oxford University Press, 122–146, https://doi.org/10.1093/acprof:oso/9780198527084.003.0008, 2005.

Hoppema, J. M. J.: The distribution and seasonal variation of alkalinity in the Southern Bight of the North Sea and in the Western Wadden Sea, Netherlands Journal of Sea Research, 26, 11–23, https://doi.org/10.1016/0077-7579(90)90053-J, 1990.

Jiang, L. Q., Cai, W. J., and Wang, Y.: A comparative study of carbon dioxide degassing in river- and marine-dominated estuaries, Limnol Oceanogr, 53, 2603–2615, https://doi.org/10.4319/lo.2008.53.6.2603, 2008.

Joesoef, A., Huang, W. J., Gao, Y., and Cai, W. J.: Air-water fluxes and sources of carbon dioxide in the Delaware Estuary: Spatial and seasonal variability, Biogeosciences, 12, 6085–6101, https://doi.org/10.5194/bg-12-6085-2015, 2015.

Kieskamp, W., Lohse, L., Epping, E., and Helder, W.: Seasonal variation in denitrification rates and nitrous oxide fluxes in intertidal sediments of the western Wadden Sea, Mar Ecol Prog Ser, 72, 145–151, https://doi.org/10.3354/meps072145, 1991.

Kitidis, V., Shutler, J. D., Ashton, I., Warren, M., Brown, I., Findlay, H., et. Al.: Winter weather controls net influx of atmospheric CO_2 on the north-west European shelf, Sci Rep, 9, https://doi.org/10.1038/s41598-019-56363-5, 2019.

Kroeker, K. J., Kordas, R. L., Crim, R., Hendriks, I. E., Ramajo, L., Singh, G. S., Duarte, C. M., and Gattuso, J. P.: Impacts of ocean acidification on marine organisms: Quantifying sensitivities and interaction with warming, Glob Chang Biol, 19, 1884–1896, https://doi.org/10.1111/gcb.12179, 2013.

Legge, O., Johnson, M., Hicks, N., Jickells, T., Diesing, M., Aldridge, J., et. al.: Carbon on the Northwest European Shelf: Contemporary Budget and Future Influences, Front Mar Sci, 7, https://doi.org/10.3389/fmars.2020.00143, 2020.

Lehmann, N., Stacke, T., Lehmann, S., Lantuit, H., Gosse, J., Mears, C., Hartmann, J., and Thomas, H.: Alkalinity responses to climate warming destabilise the Earth's thermostat, Nat Commun, 14, https://doi.org/10.1038/s41467-023-37165-w, 2023.

Lewis, E., Wallace, D., and Allison, L. J.: Program developed for CO_2 system calculations, Oak Ridge National Laboratory (ORNL), https://doi.org/10.2172/639712, 1998.

https://doi.org/10.5194/egusphere-2024-3048
Preprint. Discussion started: 23 October 2024

Li, X., Wu, Z., Ouyang, Z., and Cai, W.-J.: The source and accumulation of anthropogenic carbon in the U.S. East Coast, Sci Adv, 10, 3169, https://doi.org/10.1126/sciadv.adl3169, 2024.

Liu, Q., Dai, M., Chen, W., Huh, C. A., Wang, G., Li, Q., and Charette, M. A.: How significant is submarine groundwater discharge and its associated dissolved inorganic carbon in a river-dominated shelf system?, Biogeosciences, 9, 1777–1795, https://doi.org/10.5194/bg-9-1777-2012, 2012.

Lueker, T. J., Dickson, A. G., and Keeling, C. D.: Ocean pCO_2 calculated from dissolved inorganic carbon, alkalinity, and equations for K^1 and K^2: validation based on laboratory measurements of CO_2 in gas and seawater at equilibrium, Mar Chem, 70, 105–119, https://doi.org/10.1016/S0304-4203(00)00022-0, 2000.

Lüger, H., Wallace, D. W. R., Körtzinger, A., and Nojiri, Y.: The pCO_2 variability in the midlatitude North Atlantic Ocean during a full annual cycle, Global Biogeochem Cycles, 18, https://doi.org/10.1029/2003GB002200, 2004.

Luitjens, L.: Analytische Messung auserwählter Nährstoffkonzentrationen im ökologischen System Wattenmeer und Ems, sowie deren Entwicklung, Einflüsse und Auswirkungen, Unpublished master`s thesis, 2019.

Macovei, V. A., Petersen, W., Brix, H., and Voynova, Y. G.: Reduced Ocean Carbon Sink in the South and Central North Sea (2014–2018) Revealed From FerryBox Observations, Geophys Res Lett 48, 1–11, https://doi.org/10.1029/2021GL092645, 2021.

Norbisrath, M., Van Beusekom, J. E. E., and Thomas, H.: Distribution and source attribution of alkalinity in the Dutch Wadden Sea, Biogeosciences 20, https://doi.org/10.5194/egusphere-2023-2595, 2023.

Onken, R. and Riethmüller, R.: Determination of the freshwater budget of tidal flats from measurements near a tidal inlet, Cont Shelf Res, 30, 924–933, https://doi.org/10.1016/j.csr.2010.02.004, 2010.

Orr, J. C., Fabry, V. J., Aumont, O., Bopp, L., Doney, S. C., Feely, R. A., et. al.: Anthropogenic ocean acidification over the twenty-first century and its impact on calcifying organisms, Nature, 437, 681–686, https://doi.org/10.1038/nature04095, 2005.

Pätsch, J. and Lenhart, H.: Daily Loads of Nutrients, Total Alkalinity, Dissolved Inorganic Carbon and Dissolved Organic Carbon of the European Continental Rivers for the Years 1977-2002, Berichte Aus Dem Zentrum Für Meeres- Und Klimaforschung, Institut Für Meereskunde, 2004.

Postma, H.: Exchange of materials between the North Sea and the Wadden Sea, Mar Geol, 40, 199–213, https://doi.org/10.1016/0025-3227(81)90050-5, 1981.

Prowe, A. E. F., Thomas, H., Pätsch, J., Kühn, W., Bozec, Y., Schiettecatte, L. S., Borges, A. V., and de Baar, H. J. W.: Mechanisms controlling the air-sea CO_2 flux in the North Sea, Cont Shelf Res, 29, 1801–1808, https://doi.org/10.1016/j.csr.2009.06.003, 2009.

Redfield, A. C., Ketchum. B. H., and Richards F. A.: The influence of organisms on the composition of seawater, The sea, 2, 26–77, 1963.

Sabine, C. L., Feely, R. A., Gruber, N., Key, R. M., Lee, K., Bullister, J. L., Wanninkhof, R., Wong, C. S., Wallace, D. W. R., Tilbrook, B., Millero, F. J., Peng, T.-H., Kozyr, A., Ono, T., and Rios, A. F.: The Oceanic Sink for Anthropogenic CO_2, Science, 305, 367–371, https://doi.org/10.1126/science.1097403, 2004.

https://doi.org/10.5194/egusphere-2024-3048
Preprint. Discussion started: 23 October 2024

Santos, I. R., Beck, M., Brumsack, H. J., Maher, D. T., Dittmar, T., Waska, H., and Schnetger, B.: Porewater exchange as a driver of carbon dynamics across a terrestrial-marine transect: Insights from coupled ^{222}Rn and pCO_2 observations in the German Wadden Sea, Mar Chem, 171, 10–20, https://doi.org/10.1016/j.marchem.2015.02.005, 2015.

Schneider, A., Wallace, D. W. R., and Körtzinger, A.: Alkalinity of the Mediterranean Sea, Geophys Res Lett 34, https://doi.org/10.1029/2006GL028842, 2007.

Schulz, G., Sanders, T., Van Beusekom, J. E. E., Voynova, Y. G., Schöl, A., and Dähnke, K.: Suspended particulate matter drives the spatial segregation of nitrogen turnover along the hyper-turbid Ems estuary, Biogeosciences, 19, 2007–2024, https://doi.org/10.5194/bg-19-2007-2022, 2022.

Schwichtenberg, F.: Drivers of the Carbonate System Variability in the Southern North Sea: River Input, Anaerobic Alkalinity Generation in the Wadden Sea and Internal Processes, 2013.

Schwichtenberg, F., Pätsch, J., Böttcher, M. E., Thomas, H., Winde, V., and Emeis, K.-C.: The impact of intertidal areas on the carbonate system of the southern North Sea, Biogeosciences, 17, 4223–4245, https://doi.org/10.5194/bg-17-4223-2020, 2020.

Staneva, J., Stanev, E. V., Wolff, J. O., Badewien, T. H., Reuter, R., Flemming, B., Bartholomä, A., and Bolding, K.: Hydroynamics and sediment dynamics in the German Bight. A focus on observations and numerical modelling in the East Frisian Wadden Sea, Cont Shelf Res, 29, 302–319, https://doi.org/10.1016/j.csr.2008.01.006, 2009.

Takahashi, T., Olafsson, J., Goddard, J. G., Chipman, D. W., and Sutherland, S. C.: Seasonal variation of CO_2 and nutrients in the high-latitude surface oceans: A comparative study, Global Biogeochem Cycles, 7, 843–878, https://doi.org/10.1029/93GB02263, 1993.

Takahashi, T., Sutherland, S. C., Sweeney, C., Poisson, A., Metzl, N., Tilbrook, B., et. al.: Global sea–air CO_2 flux based on climatological surface ocean pCO_2, and seasonal biological and temperature effects, Deep Sea Research Part II: Topical Studies in Oceanography, 49, 1601–1622, https://doi.org/10.1016/S0967-0645(02)00003-6, 2002.

Talke, S. A. and De Swart, H. E.: Hydrodynamics and Morphology in the Ems/Dollard Estuary: Review of Models, Measurements, Scientific Literature, and the Effects of Changing Conditions, Institute for Marine and Atmospheric Research Utrecht, https://doi.org/http://archives.pdx.edu/ds/psu/11193, 2006.

Thomas, H., Bozec, Y., Elkalay, K., De Baar, H. J. W., Borges, A. V, and Schiettecatte, L.-S.: Controls of the surface water partial pressure of CO_2 in the North Sea, Biogeosciences, 2,323–334, https://doi.org/10.5194/bg-2-323-2005, 2005a.

Thomas, H., Bozec, Y., De Baar, H. J. W., Elkalay, K., Frankignoulle, M., Schiettecatte, L. S., Kattner, G., and Borges, A. V.: The carbon budget of the North Sea, Biogeosciences, 2, 87–96, https://doi.org/10.5194/bg-2-87-2005, 2005b.

Thomas, H., Schiettecatte, L.-S., Suykens, K., Koné, Y. J. M., Shadwick, E. H., Prowe, A. E. F., Bozec, Y., De Baar, H. J. W., and Borges, A. V: Enhanced ocean carbon storage from anaerobic alkalinity generation in coastal sediments, Biogeosciences, 6, 267–274, https://doi.org/10.5194/bg-6-267-2009, 2009.

https://doi.org/10.5194/egusphere-2024-3048
Preprint. Discussion started: 23 October 2024

Tozawa, M., Nomura, D., Nakaoka, S. ichiro, Kiuchi, M., Yamazaki, K., Hirano, D., Aoki, S., Sasaki, H., and Murase, H.: Seasonal Variations and Drivers of Surface Ocean pCO_2 in the Seasonal Ice Zone of the Eastern Indian Sector, Southern Ocean, J Geophys Res Oceans, 127, https://doi.org/10.1029/2021JC017953, 2022.

Voynova, Y. G., Petersen, W., Gehrung, M., Aßmann, S., and King, A. L.: Intertidal regions changing coastal alkalinity: The Wadden Sea-North Sea tidally coupled bioreactor, Limnol Oceanogr, 64, 1135–1149, https://doi.org/10.1002/lno.11103, 2019.

Weiss, R. F.: Carbon dioxide in water and seawater: the solubility of a non-ideal gas, Mar Chem, 2, 203–215, https://doi.org/10.1016/0304-4203(74)90015-2, 1974.

Wolf-Gladrow, D. A., Zeebe, R. E., Klaas, C., Körtzinger, A., and Dickson, A. G.: Total alkalinity: The explicit conservative expression and its application to biogeochemical processes, Mar Chem, 106, 287–300, https://doi.org/10.1016/j.marchem.2007.01.006, 2007.

Wolfstein, K., Colijn, F., and Doerffer, R.: Seasonal Dynamics of Microphytobenthos Biomass and Photosynthetic Characteristics in the Northern German Wadden Sea, Obtained by the Photosynthetic Light Dispensation System, Estuar Coast Shelf Sci, 51, 651–662, https://doi.org/10.1006/ecss.2000.0702, 2000.

Xue, L. and Cai, W. J.: Total alkalinity minus dissolved inorganic carbon as a proxy for deciphering ocean acidification mechanisms, Mar Chem, 222, https://doi.org/10.1016/j.marchem.2020.103791, 2020.

Xue, L., Cai, W. J., Sutton, A. J., and Sabine, C.: Sea surface aragonite saturation state variations and control mechanisms at the Gray's Reef time-series site off Georgia, USA (2006–2007), Mar Chem, 195, 27–40, https://doi.org/10.1016/j.marchem.2017.05.009, 2017.